UNIVERSITY OF OKLAHOMA

GRADUATE COLLEGE

NONLINEAR AMPLIFIER AMPLITUDE MODULATION DISTORTION MITIGATION TECHNIQUES

A THESIS

SUBMITTED TO THE GRADUATE FACULTY

in partial fulfillment of the requirements for the

Degree of

MASTER OF SCIENCE

By

BRIAN CARLTON

Norman, Oklahoma

2022

Downloaded from SHAREOK. Persistent Handle URL: https://hdl.handle.net/11244/335687

NONLINEAR AMPLIFIER AMPLITUDE MODULATION DISTORTION MITIGATION TECHNIQUES

A THESIS APPROVED FOR THE
SCHOOL OF ELECTRICAL AND COMPUTER ENGINEERING

BY THE COMMITTEE CONSISTING OF

Dr. Justin Metcalf, Chair

Dr. Nathan Goodman

Dr. Joeseph Havlicek

© Copyright by BRIAN CARLTON 2022

All Rights Reserved.

Acknowledgments

I owe a debt of gratitude for my mentor Dr. Justin Metcalf, who has provided extremely valuable insight into not only the technical details of the radar world (and electrical engineering in general), but also many aspects of academia and general advice that have helped me to develop into a (hopefully) much more well informed person than I was just a short year(ish) ago.

I have always regarded my time at the ARRC as a great privilege, as not only do I get to collaborate with some of the top minds of my class, but I can also draw on decades of faculty experience. This, combined with the general cool-ness of the ARRC have elevated my graduate experience to something I think is special.

I would also like to extend my gratitude to my committee members, Dr. Nathan Goodman and Dr. Joeseph Havlicek, without whom I would be short one master's degree (and very valuable insight, as well).

I would also like to thank my wife, Rylee Carlton, for her support in showing me how important my work is and, most importantly, reminding me that there indeed is a world outside school. Without her support, I think I would tend to forget that academic acomplishments are only worth something in relation to the world we live in, and in her dragging me into that world has also shown me the value of what I'm doing (along with having fun experiencing the world).

Finally, I would like to thank my family, my mom Tia Carlton, my dad (also) Brian Carlton, and my sibling AC Carlton. They have constantly shown me support

in everything I do and whether it was underwater basket weaving or rocket science, I know that they be happy for me either way (although I am happy that I get to show off something a little more impressive than underwater basket weaving).

Of course, this research could not have taken place without the generous funding I've received through the U.S. Office of Naval Research under award number N00014-20-1-2851.

Table of Contents

Acknowledgment **iv**

Table of Contents **vi**

List of Figures **ix**

Abstract **x**

1 Introduction & Outline **1**

1.1 Contributions 1

1.2 Thesis Outline 2

2 Background **4**

2.1 Amplifier Classes 4

2.1.1 Class A 4

2.1.2 Class B 5

2.2 Linearity 5

2.2.1 Fully Saturated Amplifiers 6

2.3 Linear Algrebra Concepts 7

2.3.1 Projections 8

3 Previous Techniques and Improvements **11**

3.1 Power Efficient Tandem-Hopped Radar and Communications (THoRaCs) 11

3.1.1 Spectral Shaping 12
3.1.2 Standard Complexity analysis 14
3.1.3 Frequency Domain Vector Rejection 14
3.1.4 Fast Projection and Complexity Analysis 15
3.2 Far-field Radiated Emision Design (FFRED) 16
3.2.1 Phased Arrays 16
3.2.2 Signal Model 17
3.2.3 Problem Formulation 19
3.2.4 Optimization 20
3.2.5 FFRED Frequency Domain 21
3.2.6 Efficient Frequency Domain Implementation of Gradient Descent FFRED 22
3.2.7 Complexity analysis 24

4 New Techniques **25**
4.1 Orthogonal Frequency Peak-to-average Power Ratio Reduction (OFPR) 25
4.1.1 Signal Model 25
4.1.2 Problem Formulation 26
4.1.3 Optimization 29
4.1.4 Basis Definition 32
4.1.5 Frequency Domain 32
4.1.6 Gradient Descent Version 33
4.1.7 Complexity analysis 35
4.2 Orthogonal Subspace Peak-to-average Power Ratio Reduction (OSPR) 35
4.2.1 Signal Model 35
4.2.2 Simultaneous Approach 36
4.2.3 Sequential Approach 38
4.2.4 Optimization 39
4.2.5 Frequency Domain 41

4.2.6 Complexity analysis 42

5 Results **43**

5.1 Metrics 43

5.2 OFPR 44

5.3 OFPR and FFRED 50

5.4 OSPR 52

5.5 Conclusion 59

References **61**

List of Figures

5.1 Peak-to-average Power Ratio versus $\%\beta_{\perp}$. 44
5.2 RMS Difference and Bit Error Rate vs $\%\beta_{\perp}$. 45
5.3 Peak-to-average Power Ratio versus Number of Iterations. 46
5.4 PAPR versus % Bandwidth. 47
5.5 Spectra of original and OFPR signals. 48
5.6 Spectra of original and filtered OFPR signals. 49
5.7 Efficiency of OFPR constant and non constant modulus results versus $\%\beta_{\perp}$ 51
5.8 Spatial Spectrum of FFRED. 52
5.9 Specified waveform in the time domain. 53
5.10 Spatial-temporal Spectrum of OFPR (i.e., the conventially beamformed results of OFPR). 54
5.11 Temporal spectrum of the proposed algorithms in the direction of interest. 55
5.12 Spatial spectrum of the proposed algorithms in the direction of interest. 56
5.13 Spatial-temporal spectrum of FFRED. 57
5.14 Spatial-temporal spectrum of the (frequency based) projection tensor. 57
5.15 Spatial-temporal spectrum of simultaneous OSPR. 58
5.16 Spatial-temporal spectrum of sequential OSPR. 58
5.17 PAPR reduction for each iteration of the proposed algorithms. . . . 59

Abstract

High peak-to-average power ratio (PAPR) waveforms present a challenge to radar systems in which high power amplifiers operate in saturation to increase power efficiency. Previous works have demonstrated a marked reduction in PAPR by leveraging digital arrays, namely, utilizing the spatial complement of a set of steering vectors to not interfere with RF functions. The previous work was extended by first using waveform spectral orthogonal complements to reduce PAPR, then further generalizing to n dimensional orthogonal subspace utilization, including using all avaiable degrees of freedom (time, azimuth, elevation, etc.) simultaneously or sequentially to reduce the impact in any one dimension.

Chapter 1

Introduction & Outline

One of the primary concerns of the field of radar is the total emitted power from a given aperture. Since a higher power emitted would, all things being equal, produce a higher signal-to-noise ratio (SNR), the variance of any estimation limited by SNR would decrease, resulting in higher precision estimates. However, power budgets often limit existing radar systems, especially when considering mobile systems. Therefore, it is advantageous to maximize the efficiency of a radar transmitter, as that is equivalent to maximizing the power for a given power budget, therefore increasing the precision of any estimates reliant on SNR. The primary method of increasing power emitted from radar apertures uses saturated amplifiers, a particular nonlinear amplifier case that introduces some design limitations. Developing methods to work with saturated amplifiers is crucial in increasing radar efficiency and precision.

1.1 Contributions

This thesis has the following contributions:

- Previous work, which reduced the peak-to-average power ratio (PAPR) of signals by combining two separate signals in the time domain [1, 2], or in the

spatial domain, was extended by considering the problem formulations in the temporal domain and arbitrary dimensions with a generalized signal model. The technique of alternating projections was adapted from the Far-Field Radiated Emission Design (FFRED) algorithm (the spatial domain technique) [3, 4, 5] and developed into two new algorithms: Orthogonal Subspace PAPR Reduction (OSPR) and Orthogonal Frequency PAPR Reduction (OFPR).

- A faster version of vector rejection that considers the sparsity of signals in the frequency domain was developed. This formulation reduced the complexity of the operation from quadratic to quasilinear, potentially allowing its use in real-time.

- More efficient formations of the previous algorithms were implemented using the fast vector rejection, which greatly reduced computational complexity in each case.

- The exact complexity improvement using the fast vector rejection was derived analytically for each algorithm.

- The effects of different parameters of the newly developed OSPR and the use of OFPR in conjunction with FFRED were examined.

- The efficacy of OFPR and OSPR were demonstrated on waveforms with a high PAPR.

1.2 Thesis Outline

This thesis is concerned with the effects of and use of saturated amplifiers. In particular, it is about overcoming the limitations introduced when using this am-

plifier class. The work is divided into three chapters, each focusing on a different aspect of nonlinear amplifiers. Chapter 1 investigates the rationale behind the use of saturated amplifiers. It also focuses on the nonlinear aspects of saturated amplifiers that make their use with arbitrary waveforms infeasible.

Chapter 2 gives a general overview of the concepts on which this thesis is based. Topics include the overview of amplifier use, classes of amplifiers, linearity, and nonlinear effects. Also, some linear algebra topics are discussed that underpin the algorithms developed in the following chapters.

Chapter 3 describes in detail the previous methods with which one mitigates the issues associated with the use of saturated amplifiers. It also shows the improvements of the previous work in terms of computational complexity.

Chapter 4 presents new work based on the previous work that extends it to a more general form. The previously mentioned improvements were implemented, resulting in overall more general algorithms.

In Chapter 5, the results of the previous and new works are presented for comparison. Various graphs and tables illustrate the capabilities of these algorithms (and, in the case of the last presented approach, a general framework) to reduce PAPR and ultimately facilitate the use of high PAPR waveforms with saturated waveforms.

Chapter 2

Background

2.1 Amplifier Classes

In radar systems, high power amplifiers must be employed to achieve the maximum power output. There are multiple amplifier classes than can be considered for radar applications, each with its pros and cons that determine their use as conditions dictate.

2.1.1 Class A

Perhaps the most straightforward class of amplifier, the class A amplifier uses a conduction angle of 360 degrees, ensuring that all of the information contained in the input is amplified [6]. However, because of the non-idealities of transistors, this class requires that the amplifying device be biased to conduct at all times, representing a significant power loss. The maximum efficiency of a class A amplifier is 25% efficient under normal circumstances [7]. This is because This fact severely limits class A use in radar systems, where the low power efficiency would result in low SNR and imprecise estimates.

2.1.2 Class B

The next step in amplifier efficiency is class B. This class differs from class A in that each active element (i.e., transistor) uses a conduction angle of only 180 degrees, which reduces the issue of inefficient biasing [8]. Typically, this would cause significant distortion since only half of the input signal would be used. Using a push-pull configuration, however, the associated nonlinearities with a conduction angle of 180 degrees can be reduced. This class has a maximum efficiency of $\pi/4 \approx 78\%$ [8]. The efficiency of class B makes it much more suited to and is typically employed in radar systems. However, as discussed later, this efficiency is reduced when operating in the linear region.

2.2 Linearity

The previous amplifier classes present a major trade-off in waveform design: linearity versus efficiency. While a class B amplifier is much more efficient than an equivalent class A design, the linearity is reduced. Linearity is defined as the output waveform being equivalent to the input multiplied by some constant. The primary drivers of nonlinearities in class B amplifiers are saturation nonlinearities caused by output clipping (crossover and slew rate effects also exist, but there are techniques to reduce them, such as in class AB [8]). When clipping, the output no longer equates to the input multiplied by a constant, but rather it is equal to the input multiplied by a constant when the modulus (amplitude) is less than or equal to the voltage limits, and the voltage limit otherwise. A useful metric for defining the required linearity of an amplifier is peak-to-average power ratio. The PAPR of a waveform is defined as the peak amplitude squared divided by the root mean square

of the waveform squared. The root mean square of a waveform $s(t)$ is

$$s(t)_{\text{RMS}} = \sqrt{\frac{1}{T_2 - T_1} \int_{T_1}^{T_2} |s(t)|^2 dt} \tag{2.1}$$

and the PAPR

$$\text{PAPR} = \frac{|s(t)_{\text{peak}}|^2}{s(t)_{\text{RMS}}^2} \tag{2.2}$$

Higher PAPR waveforms reduce the power output of amplifiers because of clipping, as the input must be scaled appropriately to avoid distortion. From 2.2, it is straightforward to show that the power output as a function of PAPR is

$$\text{P}_{out} = \frac{\text{P}_{max}}{\text{PAPR}}, \tag{2.3}$$

meaning that the power output is scaled by the inverse of the PAPR.

2.2.1 Fully Saturated Amplifiers

As mentioned previously, radar system design places emphasis on maximizing transmitted power and power-added efficiency. Therefore, class B is usually selected over class A operation despite the nonlinear effects. In order to achieve the highest possible output power from a class B amplifier (equivalently, in this case, highest efficiency), first note that because of clipping, the power output will scale linearly with the power input until the maximum power output is reached. This point, at which power input and output are maximized, is the most efficient point to operate, as increasing the power input further results in no increased power output. In general, waveforms transmitted through saturated amplifiers are of the form $y(t) = e^{jx(t)}$. This class of waveforms is called constant modulus since the signal's

absolute value (modulus) is constant. The PAPR of the constant modulus waveform is 1:

$$\text{PAPR} = \frac{|y(t)_{\text{peak}}|^2}{y(t)^2_{\text{RMS}}} = \frac{|1|^2}{|1|^2} = 1. \tag{2.4}$$

Therefore, when designing waveforms for saturated class B amplifiers, aim for a PAPR of 1 so that no information will be lost when clipping occurs in the amplifier.

2.3 Linear Algrebra Concepts

The concept of the orthogonal subspace comes from linear algebra, where it is known that the inner product of two length N vectors $\mathbf{a}$ and $\mathbf{b}$ is defined as

$$< \mathbf{a}, \mathbf{b} >= \sum_{i=0}^{N} a_i^* b_i = \mathbf{a}^H \mathbf{b} \tag{2.5}$$

where * represents complex conjugation. Two vectors are defined to be orthogonal if their inner product is zero. If it is the case that the vectors are elements of $\mathbb{R}^2$, then orthogonality can be considered equivalent to the lines representing the vectors being perpendicular. Two vectors that are orthogonal have the following property:

$$(\mathbf{a} + \mathbf{b})_{\text{RMS}} = \sqrt{\mathbf{a}^2_{\text{RMS}} + \mathbf{b}^2_{\text{RMS}}} \tag{2.6}$$

because, when viewing average power, which is the square of the RMS,

$$P_{\mathbf{a+b}} = (\mathbf{a}_{\text{RMS}} + \mathbf{b}_{\text{RMS}})^2 \tag{2.7}$$

$$P_{\mathbf{a+b}} = \mathbf{a}^2_{\text{RMS}} + \mathbf{b}^2_{\text{RMS}} + 2(\mathbf{ab})_{\text{RMS}} = \mathbf{a}^2_{\text{RMS}} + \mathbf{b}^2_{\text{RMS}} \tag{2.8}$$

$$(\mathbf{a} + \mathbf{b})_{\text{RMS}} = \sqrt{P_{\mathbf{a+b}}} = \sqrt{\mathbf{a}^2_{\text{RMS}} + \mathbf{b}^2_{\text{RMS}}} \tag{2.9}$$

This property will be used later when deriving powers of waveforms and orthogonal signals. Another property of orthogonal waveforms is that the projection of a vector $\mathbf{b}$ onto an orthogonal vector $\mathbf{a}$, $\mathbf{Pb}$ is the zero vector.

$$\mathbf{P} = \mathbf{a}(\mathbf{a}^H\mathbf{a})^{-1}\mathbf{a}^H \tag{2.10}$$

$$\mathbf{Pb} = \mathbf{a}(\mathbf{a}^H\mathbf{a})^{-1}\mathbf{a}^H\mathbf{b} = \mathbf{0} \tag{2.11}$$

from (2.5).

$$\mathbf{a}^H\mathbf{b} =< \mathbf{a}, \mathbf{b} >= \sum a_i b_i^* = 0^* = 0 \tag{2.12}$$

This equation also shows that orthogonal vectors have a commutative inner product even when complex (which is not the case in general), since the complex conjugate of zero is still zero.

2.3.1 Projections

The aforementioned projection matrix has a few properties worth mentioning. First of all, it is Hermitian, meaning

$$\mathbf{P} = \mathbf{P}^H \tag{2.13}$$

where $\mathbf{P}$ is a projection. Proof:

$$\mathbf{P} = \mathbf{a}(\mathbf{a}^H\mathbf{a})^{-1}\mathbf{a}^H$$

$$\mathbf{P}^H = (\mathbf{a}(\mathbf{a}^H\mathbf{a})^{-1}\mathbf{a}^H)^H = \mathbf{a}(\mathbf{a}^H\mathbf{a})^{-1}\mathbf{a}^H$$

because

$$(\mathbf{AB})^H = \mathbf{B}^H\mathbf{A}^H$$

and $(\mathbf{a}^H\mathbf{a})^{-1}$ is a scalar. This also shows that $\mathbf{P}$ is normal:

$$\mathbf{P}^H\mathbf{P} = \mathbf{P}\mathbf{P} = \mathbf{P}\mathbf{P}^H \tag{2.14}$$

The projection matrix is also idempotent:

$$\mathbf{P}^2 = \mathbf{P} = \mathbf{P}^H \tag{2.15}$$

Proof:

$$\mathbf{P}^2 = \mathbf{P}\mathbf{P} = \mathbf{a}(\mathbf{a}^H\mathbf{a})^{-1}(\mathbf{a}^H\mathbf{a})(\mathbf{a}^H\mathbf{a})^{-1}\mathbf{a}^H = \mathbf{a}(\mathbf{a}^H\mathbf{a})^{-1}\mathbf{a}^H = \mathbf{P} \tag{2.16}$$

These facts will later be used to simplify some expressions. The projection matrix is equivalent to the follwing operation:

$$\mathbf{a}_1 = \frac{\mathbf{a}\mathbf{b}^H}{\mathbf{b}\mathbf{b}^H}\mathbf{b} \tag{2.17}$$

which is the standard orthogonal projection. Another useful operation is vector rejection, which is defined as

$$\mathbf{a}_2 = \mathbf{a} - \frac{\mathbf{a}\mathbf{b}^H}{\mathbf{b}\mathbf{b}^H}\mathbf{b} \tag{2.18}$$

$$\mathbf{a}_2 = \mathbf{a} - \mathbf{a}_1$$

or equivalently

$$\mathbf{a}_2 = \mathbf{P}_\perp \mathbf{a} \tag{2.19}$$

where

$$\mathbf{P}_\perp = \mathbf{I} - \mathbf{b}(\mathbf{b}^H\mathbf{b})^{-1}\mathbf{b}^H \tag{2.20}$$

Chapter 3

Previous Techniques and Improvements

Saturating amplifiers and the associated nonlinear effects severely limit the class of waveforms used in conjunction with saturated amplifiers. However, techniques have been developed that can mitigate these effects. Approaches considered here are orthogonal subspace techniques, which make use of spectral or spatial degrees of freedom to make the overall signal constant modulus.

3.1 Power Efficient Tandem-Hopped Radar and Communications (THoRaCs)

The Power Efficient Tandem-Hopped Radar and Communications algorithm (PE-THoRaCs) [1, 2, 9], which extends the original THoRaCs framework, focuses on the simultaneous emission of a radar and communications signal from a shared aperture. Using the spectrum simultaneously for multiple purposes is of great utility to cognitive radar. Cognitive radar can be thought of in a colloquial sense as "smart" because it considers the environment in which it is operating. This can take the form of spectrum sensing and interference avoidance, whereas traditional radar systems are more static in their approaches and deal with interference more on the receive side instead of considering the source of interference and how to avoid it.

In a nutshell, cognitive radar seeks to avoid problems in the first place that traditional radar does not avoid but instead deals with directly. THoRaCs fits into this framework by providing a method to use the spectrum for both radar and comms purposes simultaneously. This intelligent use of spectrum, which is considered a limited (and changing) resource in the cognitive framework, is the primary utility of the algorithm. However, the power-efficient formulation of THoRaCs is also considered in that it not only focuses on the coexistence of radar and comms but also in that their coexistence can be constructed in such a way as to produce an overall constant modulus waveform, facilitating the use of saturated amplifiers.

3.1.1 Spectral Shaping

The first step of the THoRaCs algorithm is to generate a psudeo-random optimized frequency modulation continuous wave (PRO-FMCW) waveform [10]. The PRO-FMCW waveform starts as a constant modulus waveform with random intial phases, which can be viewed (in discretized form) as

$$\mathbf{s}_{0,m} = \exp(j\angle\mathbf{x}) \in \mathbb{C}^{N\times 1} \tag{3.1}$$

where $\mathbf{s}_{0,m}$ is the 0th iteration of the mth pulse, and $\mathbf{x}$ is a random vector such that $x_i \in \mathbf{x} \sim \mathcal{U}_{[0,2\pi]}$. This procedure generates a random vector such that $|s_i| = |s_j| \forall i, j \in [0, N-1]$ for a length N signal. In order to impose a spectral shape on this waveform one can apply the following operation:

$$\mathbf{b}_{k,m} = \mathcal{F}^{-1}\{|\mathbf{G}| \odot \exp(j\angle\mathcal{F}\{\mathbf{s}_{k,m}\})\} \in \mathbb{C}^{N\times 1} \tag{3.2}$$

where $\odot$ is the Hadamard (element-wise) product and $\mathbf{b}_{k,m}$ is the result of the kth iteration of spectral shaping of $\mathbf{s}_{k,m}$ to have the desired spectral shape of $|\mathbf{G}|^2$. After spectrally shaping the waveform, the algorithm notches the waveform, which consists of a vector rejection operation mentioned previously in (2.18).

$$\tilde{\mathbf{b}}_{k,m} = \mathbf{P}_{\perp \mathbf{r}_m} \mathbf{b}_{k,m} + \mathbf{r}_m \in \mathbb{C}^{N \times 1} \tag{3.3}$$

where $\tilde{\mathbf{b}}_{k,m}$ is the result of the kth iteration of vector rejection of $\mathbf{b}_{k,m}$ with respect to the communications signal which is to be embeded, $\mathbf{r}_m$. Here $\mathbf{P}_{\perp \mathbf{r}_m}$ is the vector rejection of $\mathbf{r}_m$, which can be written as

$$\mathbf{P}_{\perp \mathbf{r}_m} = \mathbf{I}_{N \times N} - \mathbf{r}_m (\mathbf{r}_m^H \mathbf{r}_m)^{-1} \mathbf{r}_m^H \in \mathbb{C}^{N \times N} \tag{3.4}$$

This waveform is unlikely to be constant modulus since the projection of a constant modulus signal onto a non-constant modulus signal (in this case, $\mathbf{r}_m$) is generally non-constant modulus. Therefore, the algorithm takes an additional step of making the signal constant modulus by stripping the amplitude information:

$$\mathbf{s}_{k+1,m} = \exp(j \angle \tilde{\mathbf{b}}_{k,m}) \in \mathbb{C}^{N \times 1} \tag{3.5}$$

thus resulting in the constant modulus signal $\mathbf{s}_{k+1,m}$ that represents the start of the next iteration $k+1$. The process is then repeated K times, which results in the final signal $\mathbf{s}_{K,m}$ To satisfy all constraints it is required that the sets of signals that are constant modulus, have the given spectral shape, and satisfy $\mathbf{P}_{\mathbf{r}_m} \mathbf{s}_{K,m} = \mathbf{r}_m$ all intersect.

3.1.2 Standard Complexity analysis

The most expensive operation in the THoRaCs algorithm is the vector rejection operation, which consists of multiplying the $\mathbb{C}^{N\times N}$ rejection matrix $\mathbf{P}_{\perp \mathbf{r}_m}$ with the $\mathbb{C}^{N\times 1}$ vector $\mathbf{b}_{k,m}$ resulting in an overall complexity of $O(iN^2)$ for i iterations.

3.1.3 Frequency Domain Vector Rejection

While the conventional vector rejection operation complexity is on the order of $O(N^3)$ for a vector in $\mathbb{C}^{N\times 1}$, faster techniques can reduce this complexity by instead considering the problem in the frequency domain. This is because a vector projection is simply finding the value of a such that a will minimize the distance between a vector $\mathbf{a}$ and another vector $\mathbf{a_1}$ which lies in the direction given by $\hat{\mathbf{b}} = \frac{\mathbf{b}}{||\mathbf{b}||}$

$$\min_{a} \quad ||\mathbf{a} - a\hat{\mathbf{b}}||^2 \tag{3.6}$$

The end goal of this projection is that the projected vector that is in the direction of $\mathbf{b}$. The rejection is found by subtracting the projection of $\mathbf{a}$ onto $\mathbf{b}$ from $\mathbf{a}$ (i.e. the rejection is $\mathbf{a} - \text{proj}_{\mathbf{b}}\mathbf{a}$). This results in a vector that is orthogonal to $\mathbf{b}$. Consider $\mathbf{b}$ as some $b_1\mathbf{e}_1 + b_2\mathbf{e}_2 + ...b_n\mathbf{e}_N$ for orthonormal basis vectors $\mathbf{e}_n$. A vector orthogonal to $\mathbf{b}$ can easily be found by constructing a new basis such that

$$\mathbf{f}_n = \begin{cases} \mathbf{e}_n & b_i = 0 \\ \mathbf{0}_{N\times 1} & \text{otherwise} \end{cases} \tag{3.7}$$

It follows that

$$< [\mathbf{f}_1\mathbf{f}_2...\mathbf{f}_n]\,\mathbf{a}, \mathbf{b} >= 0 \forall \mathbf{a} \tag{3.8}$$

because

$$[\mathbf{f}_1\mathbf{f}_2...\mathbf{f}_n] \odot [\mathbf{e}_1\mathbf{e}_2...\mathbf{e}_n] = \mathbf{0}_{N\times N} \tag{3.9}$$

and

$$< [\mathbf{f}_1\mathbf{f}_2...\mathbf{f}_n]\,\mathbf{a}, [\mathbf{e}_1\mathbf{e}_2...\mathbf{e}_n]\,\mathbf{b} >= \sum([\mathbf{f}_1\mathbf{f}_2...\mathbf{f}_n] \odot [\mathbf{e}_1\mathbf{e}_2...\mathbf{e}_n])\mathbf{a} \odot \mathbf{b}^* = 0 \tag{3.10}$$

where * represents complex conjugation. Now, simplify this procedure as

$$\mathbf{p} = \sum_{n=1}^{N} \mathbf{f}_n \tag{3.11}$$

and the rejection is given by

$$\mathbf{a}_2 = \mathbf{p} \odot \mathbf{a} \tag{3.12}$$

The difference between the two operations is that it is possible for there to be overlap between two orthogonal vectors ($a_i b_i \neq 0 \forall a_i, b_i \in \mathbf{a}, \mathbf{b}$) when using projection, but the fast projection only considers vectors such that $a_i b_i = 0 \forall a_i, b_i \in \mathbf{a}, \mathbf{b}$. For these algorithms, this is irrelevant because it is still possible to converge even with the fast projection. However, the overlap of the sets is reduced in this case (since the set of orthogonal vectors is reduced.)

3.1.4 Fast Projection and Complexity Analysis

In general, it is known that for every element of most signals, they are generally not equal to zero almost surely. However, different bases will have more or less zeros than the standard basis. For bandlimited signals, there are a substantial amount of zeros in the frequency domain, which enlarges the span of the orthogonal basis. Therefore the FFT is used to move the signals to the frequency domain, where the

fast projection (which is an element-wise multiply) is carried out, and moved back by the IFFT to complete the operation. The new THoRaCs algorithm becomes

$$\hat{\mathbf{b}}_{k,m} = |\mathbf{G}| \odot \exp(j\angle\mathcal{F}\{\mathbf{s}_{k,m}\}) \in \mathbb{C}^{N\times 1} \tag{3.13}$$

$$\tilde{\mathbf{b}}_{k,m} = \mathcal{F}^{-1}\{\mathbf{p}_{\perp\mathbf{r}_m} \odot \hat{\mathbf{b}}_{k,m}\} + \mathbf{r}_m \in \mathbb{C}^{N\times 1} \tag{3.14}$$

$$\mathbf{s}_{k+1,m} = \exp(j\angle\tilde{\mathbf{b}}_{k,m}) \in \mathbb{C}^{N\times 1} \tag{3.15}$$

This has effectively reduced the complexity by removing the projection matrix calculation. Now the complexity is on the order $O(iN\log N)$ since the most expensive operations are now the FFTs.

3.2 Far-field Radiated Emision Design (FFRED)

3.2.1 Phased Arrays

A phased array radar system consists of multiple discrete antenna elements arranged in some geometric pattern to form an antenna array. The phased part of the name comes from the fact that they are spaced according to the wavelength of emitted light, and by varying the phase at each element, the emission pattern can be effectively "steered" in any direction. This electronic steering is advantageous compared to traditional mechanical steering, which is limited in speed by inertia and other physical details, while only the electronics of the array limit the speed of steering for an electronic array.

Traditional active and passive electronically steered arrays (AESAs and PESAs) have a single waveform generator and are steered using analog or digital phase shifters. This is in contrast to digital arrays where, depending on the configuration,

transceivers exist at the subarray or element level. By decentralizing waveform generation, greater flexibility can be achieved in waveform transmission. The ultimate end is element-level digital arrays, where each element can be phase-shifted digitally in the waveform generator.

One of the many practical applications of digital phased arrays is the extra degrees of freedom when designing waveforms. Since each array element is equipped with a unique transceiver, any arbitrary beamforming can be achieved by digital beamforming. This opens the door to orthogonal subspace utilization, where the simultaneous access to the entire beamspace is exploited to utilize the orthogonal complement to decrease the PAPR.

The Far-field Radiated Emission Design (FFRED) algorithm proposes using this orthogonal subspace to reduce the PAPR of transmissions for digital arrays [3, 4, 5]. In particular, the FFRED algorithm was introduced to facilitate simultaneous radar and comms emissions from the same aperture. However, it can be applied to any transmission scenario in which one or more of the component waveforms are not constant modulus.

3.2.2 Signal Model

The following is the beamforming notation that will be used in the FFRED algorithm. In the far field the the emissions from a phased array will equal the following [3]

$$\sum_{m=0}^{M-1} s_m(t)\text{exp}\left(jmkd\text{sin}\theta\right) = g(t) \tag{3.16}$$

where M is the number of array elements,$d = \lambda/2$ is the spacing between elements, $s_m(t)$ is the waveform emitted by the mth element, $k = \frac{2\pi}{\lambda}$, θ is the desired angle of emission, and $g(t)$ is the desired signal at the far away point. The far field

assumption will hold for a distance $r = \frac{2D^2}{\lambda}$, the Fraunhofer distance, where D is Md, or the total size of the array. Considering the aperture of most arrays will be on the order of a decimeter (more or less) and the wavelength will be on the order of centimeters (more or less), then the Fraunhofer distance works out to be on the order of decameters. For example, a radar with aperture size $D = 50$cm operating at $f = 10$GHz will have a wavelength of $\lambda = 3$cm which implies a Fraunhofer distance of $r = \frac{2*0.5^2}{.03} = 16.7$m.

Since the systems in question are digital systems, instead of working with the continuous functions $s_m(t)$ and $g(t)$, the waveforms are discretized so that they can be represented digitally. The discrete version of (3.16) is [3]

$$\mathbf{v}^H(\theta)\mathbf{S} = \mathbf{g}^T \tag{3.17}$$

where

$$\mathbf{S} = [\mathbf{s}_0, \mathbf{s}_1, ..., \mathbf{s}_{M-1}]^T \in \mathbb{C}^{M\times N} \tag{3.18}$$

$$\mathbf{s}, \mathbf{g} \in \mathbb{C}^{N\times 1} \tag{3.19}$$

and

$$\mathbf{v}(\theta) = \left[1e^{-jkd\sin\theta}...e^{-j(M-1)kd\sin\theta}\right]^T \in \mathbb{C}^{M\times 1} \tag{3.20}$$

where N is represents the number of time samples. This formulation naturally lends itself to an extension for multiple signals in different directions. For the multi-signal scenario the matrices are constructed as [3]

$$\mathbf{C} = [\mathbf{v}(\theta_1), \mathbf{v}(\theta_2), ..., \mathbf{v}(\theta_L)] \in \mathbb{C}^{M\times L} \tag{3.21}$$

which contains the discretized spatial steering vectors for each of the L spatial an-

gles θ_l, and

$$\mathbf{G} = [\mathbf{g}_1, \mathbf{g}_2, ...\mathbf{g}_L]^T \in \mathbb{C}^{L \times N} \tag{3.22}$$

which contains the L resulting discretized far field signals. These constraints are gathered into the compact matrix representation [3]

$$\mathbf{C}^H \mathbf{S} = \mathbf{G} \tag{3.23}$$

3.2.3 Problem Formulation

With the definitions in hand, one can focus on the problem formulation, which will lead to the development of an algorithm to minimize the optimization problem. The algorithm will ideally result in a constant modulus waveform that can be transmitted without distortion through a saturated amplifier. Stated mathematically, the optimal $\mathbf{S}$ is a matrix such that (3.23) holds and the Frobenius squared norm is minimized

$$\begin{aligned} \min_{\mathbf{S}} \quad & ||\mathbf{S}||^2 \\ \text{subject to} \quad & \mathbf{C}^H \mathbf{S} = \mathbf{G} \end{aligned} \tag{3.24}$$

The solution to the optimization problem (3.24) is found directly using algebra [3]:

$$\mathbf{S}_* = \mathbf{C}(\mathbf{C}^H \mathbf{C})^{-1} \mathbf{G} \tag{3.25}$$

The resultant waveform $\mathbf{S}_*$ would indeed be the optimal solution to 3.23. However, this optimzation missed the primary requirement, which is that the waveform must be constant modulus, which for a matrix is defined as

$$|\mathbf{s}_m(n)| = |\mathbf{s}_p(q)| \forall m, p \in [0, M-1], \forall n, q \in [0, N-1] \tag{3.26}$$

Therefore the new optimization becomes

$$\begin{aligned} \min_{\mathbf{S}} \quad & ||\mathbf{S}||^2 \\ \text{subject to} \quad & \mathbf{C}^H\mathbf{S} = \mathbf{G} \\ & |\mathbf{s}_m(n)| = |\mathbf{s}_p(q)| \forall m,p \in [0, M-1], \forall n,q \in [0, N-1] \end{aligned} \tag{3.27}$$

and the solution to this optimization is the sum of the original $\mathbf{S}_*$ and a new $\mathbf{S}_\perp$ such that [3]

$$\mathbf{C}^H\mathbf{S}_\perp = \mathbf{0}_{L\times N} \tag{3.28}$$

and

$$\tilde{\mathbf{S}} = \mathbf{S}_* + \mathbf{S}_\perp = \exp\left(j\angle\tilde{\mathbf{S}}\right) \tag{3.29}$$

3.2.4 Optimization

The optimization problem can be solved using a series of alternating projections, which will be discussed in further detail later. Start with an initial constant modulus $\tilde{\mathbf{S}}_i = \alpha e^{j\angle(\mathbf{S}_*)}$. The first projection $P_A(\tilde{\mathbf{S}}_i)$, which project the signal onto the set of signals such that $\mathbf{P}\tilde{\mathbf{S}}_i = \mathbf{S}_*$, can be formulated as [3]

$$\begin{aligned} \min_{\mathbf{S_i}} \quad & ||\tilde{\mathbf{S}}_i - \mathbf{S}_i||^2 \\ \text{subject to} \quad & \mathbf{C}^H\tilde{\mathbf{S}}_i = \mathbf{G} \end{aligned} \tag{3.30}$$

The solution to (3.30) is [3]

$$\mathbf{S}_i = \mathbf{P}_\perp\tilde{\mathbf{S}}_i + \mathbf{S}_* \tag{3.31}$$

where $\mathbf{P}_\perp$ is the aforementioned orthogonal complement projection operator

$$\mathbf{P}_\perp = \mathbf{I}_{M\times M} - \mathbf{P} = \mathbf{I}_{M\times M} - \mathbf{C}(\mathbf{C}^H\mathbf{C})^{-1}\mathbf{C}^H \tag{3.32}$$

and $\mathbf{I}_{M\times M}$ is the $M \times M$ identity matrix.

The second projection, which projects the first projection into the set of constant modulus signals is represented by

$$\begin{aligned} \min_{\tilde{\mathbf{S}}_{i+1}} \quad & ||\tilde{\mathbf{S}}_{i+1} - \mathbf{S}_i||^2 \\ \text{subject to} \quad & |\tilde{\mathbf{S}}_{i+1,m,n}| = \gamma \; \forall n \in [0, N-1], \forall m \in [0, M-1] \end{aligned} \tag{3.33}$$

for some real amplitude γ. The solution to (3.33) is

$$\tilde{\mathbf{S}}_{i+1} = \gamma e^{j\angle(\mathbf{S}_i)} \tag{3.34}$$

γ, which is the sum of the squared powers of the two projections (Eq. (2.8)), can be represented as

$$\gamma = \left(\frac{\rho_*}{1 - \%\rho_\perp} \right)^{\frac{1}{2}} \tag{3.35}$$

where the two ρ are the average powers of $\mathbf{S}_*$ and $\mathbf{P}_\perp \tilde{\mathbf{S}}_i$ respectively.

3.2.5 FFRED Frequency Domain

The FFRED algorithm is subject to improvement when moving calculations to the frequency domain. As shown in section 3.2.4 FFRED algorithm consists of two projections:

$$\mathbf{S}_i = \mathbf{P}_\perp \tilde{\mathbf{S}}_i + \mathbf{S}_* \tag{3.36}$$

$$\tilde{\mathbf{S}}_{i+1} = \gamma e^{j\angle(\mathbf{S}_i)} \tag{3.37}$$

where $\mathbf{S}_i$ is an $M \times N$ matrix where each of the M rows represents an element in a phased array and each of the N columns represents a time sample. Applying the same logic as was used in developing the fast frequency implementation of

THoRaCs in section 3.1.4 results in the expressions

$$\mathbf{S}_i = \mathcal{F}^{-1}\{\hat{\mathbf{k}} \odot \mathcal{F}\{\tilde{\mathbf{S}}_i\}\} + \hat{\mathbf{S}}_* \tag{3.38}$$

$$\tilde{\mathbf{S}}_{i+1} = \gamma e^{j\angle(\mathbf{S}_i)} \tag{3.39}$$

where $\hat{\mathbf{k}}$ is an $M \times 1$ ideal frequency domain bandstop filter. For example,

$$\hat{\mathbf{k}} = [1, 1, ..., 0, ..., 1] \tag{3.40}$$

In other words, $\hat{\mathbf{k}}$ is a vector of ones with zeros placed at the desired signal location. This version removes the need to compute and store the $M \times M$ projection matrix and reduces the matrix multiply to a matrix-vector multiply. The standard matrix product is replaced with the Hadamard product to denote that $\hat{\mathbf{k}}$ should be element-wise multiplied with each column of $\mathcal{F}\{\tilde{\mathbf{S}}_i\}$. This is equivalent to the right multiplication of an $M \times M$ matrix where the diagonal is $\hat{\mathbf{k}}$, but this formulation is inefficient and defeats the purpose of moving to the frequency domain.

3.2.6 Efficient Frequency Domain Implementation of Gradient Descent FFRED

In the previous section, the solution to the optimization problem was found by considering two sets of waveforms that each individually met one of the criteria, and iteratively projecting the solution between the two sets to find the intersection. However, there are alternative methods to solve the optimzation. In particular, one may simplify the two constaints into one single cost function:[5]

$$\mathcal{J}(\gamma, \mathbf{x}) = ||\mathbf{g} - \gamma \mathbf{A}^H \exp(j\mathbf{x})||_2^2 \tag{3.41}$$

where $\mathcal{J}(\gamma, \mathbf{x})$ is the 2-norm (Euclidean) distance between the vectorized desired signal $\mathbf{g} = \text{vec}(\mathbf{G}) \in \mathbb{C}^{LN \times 1}$ and the beamformed constant modulus signal $\gamma \mathbf{A}^H \text{exp}\left(j\mathbf{x}\right) \in \mathbb{C}^{MN \times 1}$, and

$$\mathbf{A} = \mathbf{I}_{N \times N} \otimes \mathbf{C} \in \mathbb{C}^{NM \times NL}, \tag{3.42}$$

where $\otimes$ is the Kronecker product. Since the two constaints have been combined to form one cost function, the gradient descent method can now be applied to the problem. Gradient descent works by updating our optimization target (in this case, the vector $\mathbf{x}$) in the direction of fastest decrease (i.e., the gradient) of the cost function. The cost function can be solved for γ as a function of $\mathbf{x}$, which results in the following expression: [5]

$$\gamma(\mathbf{x}) = \frac{\Re\{\mathbf{g}^H \mathbf{A}^H \exp(j\mathbf{x})\}}{\|\mathbf{A}^H \exp(j\mathbf{x})\|_2^2}. \tag{3.43}$$

Then we can solve the overall expression using $\gamma(\mathbf{x})$ [5]

$$\nabla_{\mathbf{x}} \mathcal{J}(\mathbf{x}) = 2\Im\left\{\gamma(\mathbf{x}) \exp(-j\mathbf{x}) \odot \left(\mathbf{A}\left(\gamma(\mathbf{x})\mathbf{A}^H \exp(j\mathbf{x}) - \mathbf{g}\right)\right)\right\} \tag{3.44}$$

which results in a waveform $\gamma(\mathbf{x})\mathbf{A}^H \text{exp}\left(j\mathbf{x}\right)$ that meets the criteria. However, using the Kronecker product is inefficent and the algorithm can be simplified as

$$\gamma(\mathbf{X}) = \frac{\Re\{\sum\left(\mathbf{C}^* \mathbf{G}^* \odot \exp(j\mathbf{X})\right)\}}{\|\mathbf{C}^H \exp(j\mathbf{X})\|_F^2}. \tag{3.45}$$

$$\nabla_{\mathrm{X}} \mathcal{J}(\mathrm{X}) = 2\Im\left\{\gamma(\mathrm{X}) \exp(-j\mathrm{X}) \odot \left(\mathbf{C}\left(\gamma(\mathrm{X})\mathbf{C}^H \exp(j\mathrm{X}) - \mathrm{G}\right)\right)\right\} \tag{3.46}$$

3.2.7 Complexity analysis

The various implementations of the FFRED algorithm have various complexities. Starting with the initially proposed FFRED algorithm, the computational complexity of the multiplication of the projection matrix $\mathbf{P}_{\perp} \in \mathbb{C}^{M \times M}$ with $\mathbf{S} \in \mathbb{C}^{M \times N}$ is on the order $O(M^2 N)$ using traditional matrix multiply, or, if $M \approx N$, $O(N^3)$, giving an overall complexity $O(iN^3)$ for i iterations. In the frequency domain formulation the most expensive computation is $\mathbf{S}_*$, which comes to $O(iM^2 L) \approx O(N^2), L << M$ when considering $\mathbf{C}(\mathbf{C}^H\mathbf{C})^{-}1\mathbf{G}$ as equivalent to $(\mathbf{C}^H)^{+}\mathbf{G}$, where $^+$ is the pseudoinverse. When the angle is not changing, this is a one-time calculation, meaning that in the long run, the complexity is closer to $O(iN\log N)$, which is the complexity of the FFTs.

Chapter 4

New Techniques

4.1 Orthogonal Frequency Peak-to-average Power Ratio Reduction (OFPR)

The previous techniques considered temporal orthogonal subspaces (THoRaCs) and spatial orthogonal subspaces (FFRED). However, in each case, the original focus of the algorithm design was on dual radar comms functionality. These ideas can be expanded to more general cases, first in the temporal case, then in general for any number of dimensions. The Orthogonal Frequency Peak-to-average Power Ratio Reduction (OFPR) algorithm, discussed first, will be based on FFRED in that it uses two alternating projections that produce a constant modulus signal with given desired characteristics but operates in the temporal/spectral dimension.

4.1.1 Signal Model

Let the desired transmitted signal be represented as a bandlimited discrete finite signal given by a length $N \times 1$ vector $\mathbf{r}$, such that

$$r[n] = \sum_{b=0}^{B-1} |c_b| e^{-j2\pi f_b \frac{n}{N} + \angle c_b} \tag{4.1}$$

Equivalently,

$$\mathbf{r} = \sum_{b=0}^{B-1} \mathbf{v}(f_b) c_b \tag{4.2}$$

where

$$\mathbf{v}(f) = [1, e^{-j\phi_\Delta f}, e^{-j2\phi_\Delta f}, ..., e^{-j(N-1)\phi_\Delta f}]^T \tag{4.3}$$

is an $N \times 1$ frequency vector and $\phi_\Delta = \frac{2\pi}{N}$.

Equation (4.3) can then be simplified as the matrix operation

$$\mathbf{r} = \mathbf{D}\mathbf{c} \tag{4.4}$$

where $\mathbf{D} = [\mathbf{v}(f_0)\ \mathbf{v}(f_1)\ ...\ \mathbf{v}(f_B)]$ is an $N \times B$ underspecified DFT matrix and $\mathbf{c} = [c_0, c_1, ..., c_B]$ is a $B \times 1$ vector of complex frequency coefficients.

4.1.2 Problem Formulation

Because of the limitations of nonlinear amplifiers, OFPR will ideally result in some signal $\mathbf{s}$ that is equivalent to $\mathbf{r}$ within its bandwidth, yet is also constant modulus. In general, some $\tilde{\mathbf{r}}$ which is not necessarily bandlimited, but contains no useful information outside of the bandwidth of interest will still suffice. Therefore $\tilde{\mathbf{r}}$ may be expressed as

$$\tilde{\mathbf{r}} = \mathbf{D}\mathbf{c} + \mathbf{D}_\perp \mathbf{c}_\perp \tag{4.5}$$

where $\mathbf{D}_\perp \mathbf{c}_\perp$ represents all frequency content outside of the relevant bandwidth.

The problem can be formulated as

$$\begin{aligned} \min_{\mathbf{s}} \quad & ||\mathbf{s}||^2 \\ \text{subject to} \quad & \mathbf{Ps} = \mathbf{r} \\ & \mathbf{s} = \alpha e^{j\angle\theta_n} \end{aligned} \tag{4.6}$$

where $\mathbf{P}$ is the orthogonal projection operator

$$\mathbf{P} = \mathbf{D}\mathbf{D}^{+} \tag{4.7}$$

and $^{+}$ represents the Moore-Penrose inverse, which in this case is computed using singular value decomposition since $\mathbf{D}$ is not full rank.

It can be shown that the minimum norm solution $\mathbf{s}_*$ to (4.6) is

$$\mathbf{s}_* = \tilde{\mathbf{r}} \tag{4.8}$$

as $\mathbf{P}\tilde{\mathbf{r}} = \mathbf{D}\mathbf{D}^{+}\mathbf{D}\mathbf{c} + \mathbf{D}\mathbf{D}^{+}\mathbf{D}_{\perp}\mathbf{c}_{\perp} = \mathbf{D}\mathbf{c} = \mathbf{r}$. due to the properties of the pseudoinverse. $\mathbf{D}\mathbf{D}^{+}\mathbf{D}_{\perp}\mathbf{c}_{\perp}$ is the zero vector because $\mathbf{D}_{\perp}$ is orthogonal to $\mathbf{D}$ and therefore the projection of $\mathbf{D}_{\perp}$ onto $\mathbf{D}$ is the zero matrix.

The first constraint enforces that $\mathbf{s}_*$ is equal to $\mathbf{r}$ in the relevant bandwidth defined by $\mathbf{D}$. However, it does not satisfy the constant modulus constraint. As $\mathbf{s}$ and $\mathbf{r}$ must be equal across the bandwidth of interest for the first constraint to be satisfied, the spectrum outside of the relevant bandwidth must be used to make $\mathbf{s}$ constant modulus.

In order to satisfy both constraints, the null space of $\mathbf{D}$ will be used to form

some vector $\mathbf{s}_\perp$ which is orthogonal to $\mathbf{s}_*$ such that

$$\tilde{\mathbf{s}} = \mathbf{s}_* + \mathbf{s}_\perp \tag{4.9}$$

where $\mathbf{s}_*$ is the non-constant modulus minimum norm solution satisfying (4.6), and $\mathbf{s}_\perp$ is an $N \times 1$ vector such that

$$\mathbf{P}\mathbf{s}_\perp = \mathbf{0} \tag{4.10}$$

and $\mathbf{s}_* + \mathbf{s}_\perp$ add up to a constant modulus signal

$$\mathbf{s}_* + \mathbf{s}_\perp = \alpha e^{j\angle\theta_n} \tag{4.11}$$

where α represents some constant amplitude. Because $\mathbf{s}_*$ and $\mathbf{s}_\perp$ are orthogonal, the average power of $\tilde{\mathbf{s}}$, represented by α, is simply

$$\alpha^2 = \beta_* + \beta_\perp \tag{4.12}$$

where β_* and $\beta_\perp$ are the average powers of $\mathbf{s}_*$ and $\mathbf{s}_\perp$, respectively, defined by

$$\beta_* = \frac{1}{N}||\mathbf{s}_*||^2 \tag{4.13}$$

and

$$\beta_\perp = \frac{1}{N}||\mathbf{s}_\perp||^2 \tag{4.14}$$

As the solution $\mathbf{s}_*$ is optimal and therefore constant, a change in α represents a change in the power of the orthogonal signal. The percent of the power that the

orthogonal subspace occupies is

$$\%\beta_{\perp} = \frac{\beta_{\perp}}{\alpha^2} \times 100\% \tag{4.15}$$

As this power does not contribute to the actual signal being sent, this power is wasted in the sense that it does not contribute to the transfer of data. However, it still can serve as illumination for simultaneous radar comms. For communications, $\%\beta_{\perp}$ is a measure of efficiency. By varying $\%\beta_{\perp}$, the amount of power that is put into the orthogonal complement is varied, affecting the degree to which the constant modulus constraint can be satisfied.

4.1.3 Optimization

It has been shown [4] that a series of alternating projections will satisfy both constraints of (4.6) (given that the intersection of the two sets exists). The algorithm works by first projecting $\tilde{\mathbf{s}}_0$ into the vector space containing solutions to the first constraint. Next, $\mathbf{s}_i$ is projected into the vector space of constant modulus signals. The space of all constant modulus signals is non-convex; therefore, one must use an iterative process to converge to a solution satisfying the constraints. This process is a modification of the projection onto convex sets (POCS) algorithm [11, 12] into the error reduction algorithm (ERA) because the second projection is onto a non-convex set [4, 13, 14, 15, 16]. Using the error reduction algorithm framework, the resulting algorithm will be of the form

$Initialize : \tilde{\mathbf{s}}_0, i = 0$

repeat

$\mathbf{s}_i = P_A(\tilde{\mathbf{s}}_i)$

$\tilde{\mathbf{s}}_{i+1} = P_B(\mathbf{s}_i)$

$i = i + 1$

until converged

where the algorithm will alternate between two projections until some convergence criteria is met.

Start with an initial constant modulus $\tilde{\mathbf{s}}_i = \alpha e^{j\angle(\mathbf{s}_i)}$. The first projection $P_A(\tilde{\mathbf{s}}_i)$, which will enforce the signal constraint, can be formulated as

$$\begin{aligned} \min_{\mathbf{s_i}} \quad & ||\tilde{\mathbf{s}}_i - \mathbf{s}_i||^2 \\ \text{subject to} \quad & \mathbf{P}\mathbf{s}_i = \mathbf{r} \end{aligned} \tag{4.16}$$

The solution to (4.16) is

$$\mathbf{s}_i = \mathbf{P}_\perp \tilde{\mathbf{s}}_i + \mathbf{s}_* \tag{4.17}$$

where $\mathbf{P}_\perp$ is the orthogonal complement projection operator

$$\mathbf{P}_\perp = \mathbf{I}_{N\times N} - \mathbf{P} = \mathbf{I}_{N\times N} - \mathbf{D}\mathbf{D}^+ \tag{4.18}$$

and $\mathbf{I}_{N\times N}$ is the $N \times N$ identity matrix.

The second projection, which projects the first projection into the set of constant modulus signals, in this case $\alpha e^{j\angle\theta}$, where $\angle(\cdot)$ represents the phase of the argument, is represented by

$$\begin{aligned} \min_{\tilde{\mathbf{s}}_{i+1}} \quad & ||\tilde{\mathbf{s}}_{i+1} - \mathbf{s}_i||^2 \\ \text{subject to} \quad & |\tilde{\mathbf{s}}_{i+1}(n)| = \alpha \; \forall n \in [0, N-1] \end{aligned} \tag{4.19}$$

for some real amplitude α. The solution to (4.19) is

$$\tilde{\mathbf{s}}_{i+1} = \alpha e^{j\angle(\mathbf{s}_i)} \tag{4.20}$$

From (4.15), it is known that α, which is the sum of the squared powers of the two projections, can be represented as

$$\alpha = \left(\frac{\beta_*}{1 - \%\beta_\perp} \right)^{\frac{1}{2}} \tag{4.21}$$

After reaching some convergence criteria, if the two sets intersect, a solution is found. Otherwise, one can choose between either taking the result of the first or second projection. If the two sets do not intersect, then it is unlikely that the constant modulus solution will be equal to $\mathbf{r}$ across its bandwidth.

If other methods such as FFRED [4] can further reduce the PAPR, then one should take the answer as $\mathbf{s}_i$ to avoid distortion and signal degradation. The result will be the signal with extra power in orthogonal frequencies to reduce the PAPR. However, if the system is not a phased array, then the answer should be taken as $\tilde{\mathbf{s}}_i$ since that result will always be constant modulus.

By varying $\%\beta_\perp$, it is determined how much of the power of our signal is put into the orthogonal frequencies. By placing more power in this part of the spectrum, it becomes more likely that the two sets will intersect, and therefore, the solution will be both constant modulus and equal to $\mathbf{r}$ across its bandwidth. However, by increasing $\%\beta_\perp$, the relative power of the communications signal is decreased. Therefore a trade-off emerges between a high enough $\%\beta_\perp$ guaranteeing the intersection of the two solution spaces and a low enough $\%\beta_\perp$ that keeps enough power in $\mathbf{r}$ as to represent an overall increase in efficiency by allowing high power amplifiers to operate in saturation mode. Unlike the case of [4], the OFPR algorithm has a second design degree of freedom - the dimension of the bandwidth used for the signal. For a given $\%\beta_\perp$, OFPR will reduce the PAPR more for larger allowed bandwidth, shown later in Chapter 5.

4.1.4 Basis Definition

When defining $\mathbf{D}$, the natural choice is to use all the frequencies that make up the bandwidth of the signal of interest and leave the rest for OFPR to use in reducing the PAPR. However, one would like to limit the total bandwidth of the signal. Let $a \in \mathbb{Z}$ such that

$$\tilde{\mathbf{f}} = \{f | f \in \mathbf{f} \text{ or } f \pm a = N/2\} \tag{4.22}$$

where $\mathbf{f}$ is the set of frequencies that determine $\mathbf{r}$, and $\tilde{\mathbf{f}}$ is a $\tilde{B} \times 1$ vector of new frequencies. a represents the so called "guard window," much like in communications, that is set aside and reserved so that no extra power is placed in the window. By placing the window around $N/2$, the total bandwidth of the signal is limited. From $\tilde{\mathbf{f}}$, construct $\mathbf{D}$

$$\mathbf{D} = [\mathbf{v}(\tilde{f}_0)\ \mathbf{v}(\tilde{f}_1)\ ...\ \mathbf{v}(\tilde{f}_{\tilde{B}})] \tag{4.23}$$

where $\tilde{f}_i$ is the ith element of $\tilde{\mathbf{f}}$.

4.1.5 Frequency Domain

As the OFPR algorithm works by placing extra power in the unused bandwidth of a signal, the operation $\mathbf{P}_{\perp}\tilde{\mathbf{s}}_i$ can be viewed as a form of bandpass filtering. Therefore, instead of the expensive matrix vector multiply, fast Fourier transforms (FFTs) are used to do this filtering in the frequency domain. Let $\hat{\mathbf{g}}$ be a length N spectral shape vector such that

$$\hat{\mathbf{g}}(\tilde{\mathbf{f}}) = 0,\ 1 \text{ otherwise} \tag{4.24}$$

Substituting $\mathbf{g}$ for $\mathbf{P}$ yields

$$\mathbf{s}_i = \mathbf{g} * \tilde{\mathbf{s}}_i + \mathbf{s}_*, \tag{4.25}$$

where $*$ is the convolution operation. Taking the discrete Fourier transform (DFT) of the former equation yields

$$\hat{\mathbf{s}}_i = \hat{\mathbf{g}} \cdot \hat{\tilde{\mathbf{s}}}_i + \hat{\mathbf{s}}_* \tag{4.26}$$

because of the convolution theorm. This leads to the modified algorithm

$$\mathbf{s}_i = \mathcal{F}^{-1}\{\hat{\mathbf{g}} \cdot \mathcal{F}\{\tilde{\mathbf{s}}_i\}\} + \mathbf{s}_* \tag{4.27}$$

$$\tilde{\mathbf{s}}_{i+1} = \alpha e^{j\angle(\mathbf{s}_i)} \tag{4.28}$$

Because there is no matrix-vector multiplication in this algorithm, it will be faster than the previous version. Also, with the removal of $\mathbf{P}$, which is size N^2, the storage requirements will be significantly reduced.

4.1.6 Gradient Descent Version

From [5], the optimization problem (4.6) can be equivalently stated as

$$\begin{aligned} \min_{\alpha,\mathbf{x}} \quad & \alpha^2 \\ \text{subject to} \quad & \alpha \mathbf{P} e^{j\mathbf{x}} = \mathbf{r} \end{aligned} \tag{4.29}$$

and a relaxed form as

$$\min_{\tilde{\alpha},\tilde{\mathrm{x}}} \mathcal{J}(\tilde{\alpha}, \tilde{\mathrm{x}}) = \|\tilde{\alpha}\mathbf{P}e^{j\tilde{\mathbf{x}}} - \mathbf{r}\|^2 \tag{4.30}$$

Solving for $\tilde{\alpha}$ in terms of $\tilde{\mathbf{x}}$ yields

$$\tilde{\alpha}(\tilde{\mathbf{x}}) = \frac{\Re\{\mathbf{r}^H \mathbf{P} e^{j\tilde{\mathbf{x}}}\}}{\|\mathbf{P}e^{j\tilde{\mathbf{x}}}\|^2} \tag{4.31}$$

Inserting this into the previous equation yields

$$\mathcal{J}(\tilde{\alpha}(\tilde{\mathbf{x}}),\tilde{\mathbf{x}}) = \tilde{\mathcal{J}}(\tilde{\mathbf{x}}) = \|\mathbf{r}\|^2 - \frac{\left(\Re\{\mathbf{r}^H\mathbf{P}e^{j\tilde{\mathbf{x}}}\}\right)^2}{||\mathbf{P}e^{j\tilde{\mathbf{x}}}||^2}. \tag{4.32}$$

The gradient of the cost function with respect to $\tilde{\mathbf{x}}$ is

$$\nabla_{\overline{\mathbf{x}}}\widetilde{\mathcal{J}}\left(\widetilde{\mathbf{x}}\right) = 2\Im\left\{\tilde{\alpha}\left(\widetilde{\mathbf{x}}\right)e^{-j\widetilde{\mathbf{x}}}\cdot\left(\mathbf{P}^H\left(\tilde{\alpha}\left(\widetilde{\mathbf{x}}\right)\mathbf{P}e^{j\widetilde{\mathbf{x}}}-\mathbf{r}\right)\right)\right\} \tag{4.33}$$

and because $\mathbf{P}$ is unitary, it can be reduced to

$$\nabla_{\overline{\mathbf{x}}}\widetilde{\mathcal{J}}\left(\widetilde{\mathbf{x}}\right) = 2\tilde{\alpha}\left(\widetilde{\mathbf{x}}\right)\Im\left\{e^{-j\widetilde{\mathbf{x}}}\cdot\left(\mathbf{P}\left(\tilde{\alpha}\left(\widetilde{\mathbf{x}}\right)e^{j\widetilde{\mathbf{x}}}-\mathbf{r}\right)\right)\right\} \tag{4.34}$$

The benefit to using this form of the algorithm is that the answer will always be optimal in the sense that the difference between $\mathbf{P}e^{j\mathbf{x}}$ and $\mathbf{r}$ will be minimized as well as the power outside of the usable bandwidth. This form can be thought of as always choosing the "correct" value of $\%\beta_\perp$ that is the smallest possible value that leads to a minimized error. From the previous section, modify the gradient descent algorithm by performing filtering in the frequency domain. First, define $\hat{\mathbf{s}}$ as

$$\hat{\mathbf{s}} = \mathcal{F}\left\{e^{j\widetilde{\mathbf{x}}}\right\} \tag{4.35}$$

The new gradient descent algorithm becomes

$$\nabla_{\overline{\mathbf{x}}}\widetilde{\mathcal{J}}\left(\widetilde{\mathbf{x}}\right) = 2\tilde{\alpha}\left(\widetilde{\mathbf{x}}\right)\Im\left\{e^{-j\widetilde{\mathbf{x}}}\cdot\mathcal{F}^{-1}\left\{\hat{\mathbf{g}}\cdot\left(\tilde{\alpha}\left(\widetilde{\mathbf{x}}\right)\hat{\mathbf{s}}-\hat{\mathbf{r}}\right)\right\}\right\} \tag{4.36}$$

α can be written as

$$\tilde{\alpha}(\tilde{\mathbf{x}}) = \frac{\Re\{\mathbf{r}^H\mathcal{F}^{-1}\{\hat{\mathbf{g}}\hat{\mathbf{s}}\}\}}{\|\mathcal{F}^{-1}\{\hat{\mathbf{g}}\hat{\mathbf{s}}\}\|^2} \tag{4.37}$$

4.1.7 Complexity analysis

The most expensive operation in the OFPR algorithm is the projection $\mathbf{P}_{\perp}\tilde{\mathbf{s}}_i$, which is $O(N^2)$. Therefore the overall complexity of the algorithm is $O(iN^2)$, where i is the number of iterations. This is also the case for the gradient descent version. By doing work in the frequency domain, the matrix-vector multiply is removed, and the most expensive operations become the FFTs, which are $O(NlogN)$, giving an overall complexity of $O(iNlogN)$ for both the regular and gradient descent versions.

4.2 Orthogonal Subspace Peak-to-average Power Ratio Reduction (OSPR)

OFPR extended the FFRED to the temporal dimension and, in doing so, showed that it applies to any dimension in which degrees of freedom are available. This leads naturally to the development of an even more general algorithm: Orthogonal Subspace Peak-to-Average Power Ratio Reduction (OSPR). Instead of only working on one dimension, such as space or time, the OSPR algorithm works on all available dimensions. For rectangular phased arrays, which beamform in azimuth and elevation, there are three dimensions available to place extra power.

4.2.1 Signal Model

Let our general discretized signal be a rank N tensor of the form

$$\mathbf{r} = \mathbf{v}_1 \otimes \mathbf{v}_2 \otimes ... \otimes \mathbf{v}_N \tag{4.38}$$

where each $\mathbf{v}_n$ represents the desired signal in dimension n. Each $\mathbf{v}_n$ is size t_n, meaning that the overall dimensions of $\mathbf{r}$ are $t_1 \times t_2 \times ...t_n$. This representation can balloon very quickly. Considering each t_n to be on the same order, the size of the tensor would be on the order of $O(t_n^N)$, which shows that just the size of the tensors in question grow exponentially. Therefore, it is advantageous to consider another operating regime in which the OSPR algorithm is applied sequentially across the different dimensions of the array. This will benefit from being much faster, at the cost of any coupled effects between dimensions.

4.2.2 Simultaneous Approach

As before, the problem can be formulated as

$$\begin{aligned} \min_{\mathbf{s}} \quad & ||\mathbf{s}||^2 \\ \text{subject to} \quad & \mathbf{P}\mathbf{s} = \mathbf{r} \\ & \mathbf{s} = \alpha e^{j\angle\theta_n} \end{aligned} \tag{4.39}$$

where $\mathbf{P}$ is the orthogonal projection operator

$$\mathbf{P} = \mathbf{r}\mathbf{r}^{+} \tag{4.40}$$

The minimum norm solution $\mathbf{s}_*$ to (4.39) is

$$\mathbf{s}_* = \mathbf{r} \tag{4.41}$$

The first constraint enforces that $\mathbf{P}\mathbf{s}_* = \mathbf{r}$. To satisfy the second constraint, the orthogonal subspace of $\mathbf{r}$ will be used to form some tensor $\mathbf{s}_\perp$ which is orthogonal

to $\mathbf{s}_*$ such that

$$\tilde{\mathbf{s}} = \mathbf{s}_* + \mathbf{s}_\perp \tag{4.42}$$

where $\mathbf{s}_*$ is the non-constant modulus minimum norm solution satisfying (4.6), $\mathbf{s}_\perp$ is an $t_1 \times t_2 \times ... \times t_N$ tensor, and $\mathbf{s}_* + \mathbf{s}_\perp$ add up to a constant modulus signal

$$\mathbf{s}_* + \mathbf{s}_\perp = \alpha e^{j\angle\theta_{1,2,3...N}} \tag{4.43}$$

where α represents some constant amplitude. Because $\mathbf{s}_*$ and $\mathbf{s}_\perp$ are orthogonal, the average power of $\tilde{\mathbf{s}}$, represented by α, is simply

$$\alpha^2 = \beta_* + \beta_\perp \tag{4.44}$$

where β_* and $\beta_\perp$ are the average powers of $\mathbf{s}_*$ and $\mathbf{s}_\perp$, respectively, defined by

$$\beta_* = \frac{1}{t_1 t_2 ... t_N} ||\mathbf{s}_*||^2 \tag{4.45}$$

and

$$\beta_\perp = \frac{1}{t_1 t_2 ... t_N} ||\mathbf{s}_\perp||^2 \tag{4.46}$$

As the solution $\mathbf{s}_*$ is optimal and therefore constant, a change in α represents a change in the power of the orthogonal signal.

$$\%\beta_\perp = \frac{\beta_\perp}{\alpha^2} \times 100\% \tag{4.47}$$

is the percentage of total signal power that the orthogonal signal takes up.

4.2.3 Sequential Approach

Instead of forming our tensor $\mathbf{r}$ and applying the OSPR algorithm all at once, instead, operate sequentially across the different dimensions to greatly reduce complexity. Each step will operate on $\mathbf{v}_n$, a size $t_n \times 1$ vector, rather than $\mathbf{r}$.

$$\begin{aligned} \min_{\mathbf{s}_n} \quad & ||\mathbf{s}_n||^2 \\ \text{subject to} \quad & \mathbf{P}_n \mathbf{s}_n = \mathbf{v}_n \\ & \mathbf{s}_n = \alpha e^{j\angle\theta_n} \end{aligned} \tag{4.48}$$

where $\mathbf{P}_n$ is the orthogonal projection operator for the vector under consideration

$$\mathbf{P}_n = \mathbf{v}_n \mathbf{v}_n^+ \tag{4.49}$$

The minimum norm solution $\mathbf{s}_*$ to (4.48) is as before

$$\mathbf{s}_{*n} = \mathbf{v}_n \tag{4.50}$$

To satisfy the second constraint, the orthogonal subspace of $\mathbf{v}_n$ will be used to form some vector $\mathbf{s}_{\perp n}$ which is orthogonal to $\mathbf{s}_{*n}$ such that

$$\tilde{\mathbf{s}}_n = \mathbf{s}_{*n} + \mathbf{s}_{\perp n} \tag{4.51}$$

where $\mathbf{s}_*$ is the non-constant modulus minimum norm solution satisfying (4.48), $\mathbf{s}_{\perp n}$ is a $t_n 1$ vector, and $\mathbf{s}_{*n} + \mathbf{s}_{\perp n}$ add up to a constant modulus signal

$$\mathbf{s}_{*n} + \mathbf{s}_{\perp n} = \alpha e^{j\angle\theta_n} \tag{4.52}$$

where α represents some constant amplitude. Because $\mathbf{s}_{*n}$ and $\mathbf{s}_{\perp n}$ are orthogonal, the average power of $\tilde{\mathbf{s}}$ is

$$\alpha^2 = \beta_* + \beta_\perp \tag{4.53}$$

where β_* and $\beta_\perp$ are the average powers of $\mathbf{s}_{*n}$ and $\mathbf{s}_{\perp n}$, respectively, defined by

$$\beta_* = \frac{1}{t_n}||\mathbf{s}_{*n}||^2 \tag{4.54}$$

and

$$\beta_\perp = \frac{1}{t_n}||\mathbf{s}_{\perp n}||^2 \tag{4.55}$$

As the solution $\mathbf{s}_*$ is optimal and therefore constant, a change in α represents a change in the power of the orthogonal signal.

$$\%\beta_\perp = \frac{\beta_\perp}{\alpha^2} \times 100\% \tag{4.56}$$

is the percentage of total signal power that the orthogonal signal takes up.

4.2.4 Optimization

When using either the simultaneous or sequential approach, the algorithm will look the same, except that in the simultaneous case the algorithm will be operating over the entire tensor at once, while the sequential approach will be applied to each dimension separately. Using the error reduction algorithm framework, the algorithm will be of the form

$Initialize : \tilde{\mathbf{s}}_0, i = 0$

repeat

$\mathbf{s}_i = P_A(\tilde{\mathbf{s}}_i)$

$\tilde{\mathbf{s}}_{i+1} = P_B(\mathbf{s}_i)$

$i = i + 1$

until converged

where the algorithm will alternate between two projections until some convergence criteria is met.

The rest of the notation will be for the simultaneous case; the sequential case would add the $_n$ subscript as appropriate. Start, as before, with an initial constant modulus $\tilde{\mathbf{s}}_i = \alpha e^{j\angle(\mathbf{s}_i)}$. The first projection $P_A(\tilde{\mathbf{s}}_i)$, which will enforce the signal constraint, can be formulated as

$$\begin{aligned} \min_{\mathbf{s_i}} \quad & ||\tilde{\mathbf{s}}_i - \mathbf{s}_i||^2 \\ \text{subject to} \quad & \mathbf{P}\mathbf{s}_i = \mathbf{r} \end{aligned} \tag{4.57}$$

The solution to (4.57) is

$$\mathbf{s}_i = \mathbf{P}_\perp \tilde{\mathbf{s}}_i + \mathbf{s}_* \tag{4.58}$$

where $\mathbf{P}_\perp$ is the orthogonal complement projection operator

$$\mathbf{P}_\perp = \mathbf{I}_{N\times N} - \mathbf{P} = \mathbf{I}_{t_1\times t_2\times \ldots t_n} - \mathbf{r}\mathbf{r}^+ \tag{4.59}$$

and $\mathbf{I}_{N\times N}$ is the $N \times N$ identity tensor.

The second projection, which projects the first projection into the set of constant modulus tensors, in this case $\alpha e^{j\angle\theta}$, where $\angle(\cdot)$ represents the phase of the argument, is represented by

$$\begin{aligned} \min_{\tilde{\mathbf{s}}_{i+1}} \quad & ||\tilde{\mathbf{s}}_{i+1} - \mathbf{s}_i||^2 \\ \text{subject to} \quad & |\tilde{\mathbf{s}}_{i+1}(1, 2, 3 \ldots N)| = \alpha \end{aligned} \tag{4.60}$$

for some real amplitude α. The solution to (4.60) is

$$\tilde{\mathbf{s}}_{i+1} = \alpha e^{j\angle(\mathbf{s}_i)} \tag{4.61}$$

From (4.47), it is known that α, which is the sum of the squared powers of the two projections, can be represented as

$$\alpha = \left(\frac{\beta_*}{1 - \%\beta_\perp} \right)^{\frac{1}{2}} \tag{4.62}$$

Using the sequential version of the OSPR algorithm will result in N vectors that must be combined to form the final tensor as

$$\tilde{\mathbf{s}} = \tilde{\mathbf{s}}_1 \otimes \tilde{\mathbf{s}}_2 \otimes ... \otimes \tilde{\mathbf{s}}_N \tag{4.63}$$

4.2.5 Frequency Domain

The same frequency domain improvements as before can be applied to OSRP. Let $\hat{\mathbf{g}}_n$ be a length t_n spectral shape vector such that

$$\hat{\mathbf{g}}_n = [1, 1, ..., 0, ..., 1] \tag{4.64}$$

Where the number and placement of zeros depends on the dimension. Substituting $\mathbf{g}$ for $\mathbf{P}$ and taking the discrete Fourier transform (DFT) of the former equation yields

$$\mathbf{s}_{i,n} = \mathcal{F}^{-1}\{\hat{\mathbf{g}}_n \cdot \mathcal{F}\{\tilde{\mathbf{s}}_{i,n}\}\} + \mathbf{s}_{*\mathbf{n}} \tag{4.65}$$

$$\tilde{\mathbf{s}}_{i+1,n} = \alpha e^{j\angle(\mathbf{s}_{i,n})} \tag{4.66}$$

For the simultaneous version:

$$\mathbf{s}_i = \mathcal{F}^{-1}\{\hat{\mathbf{g}} \cdot \mathcal{F}\{\tilde{\mathbf{s}}_i\}\} + \mathbf{s}_* \tag{4.67}$$

$$\tilde{\mathbf{s}}_{i+1} = \alpha e^{j\angle(\mathbf{s}_i)} \tag{4.68}$$

where

$$\hat{\mathbf{g}} = \hat{\mathbf{g}}_1 \otimes \hat{\mathbf{g}}_2 \otimes ...\hat{\mathbf{g}}_N \tag{4.69}$$

4.2.6 Complexity analysis

The most expensive operation in the simultaneous OSPR algorithm is the projection $\mathbf{P}_\perp \tilde{\mathbf{s}}_i$ which is $O((t_1 t_2 ... t_n)^2) \approx O(it^{2N})$ for i iterations, which, depending on N and t could be very large. For the frequency domain formulation, this becomes approximately $O(it^N \log t^N)$, which is slightly more manageable. In the sequential version, the algorithm has a complexity on the order $O(it^2)$ for each dimension, giving an overall complexity of $O(Nit^2)$, which is far less complex than the simultaneous version. For the frequency domain formulation, the overall complexity is $O(Nit \log t)$. Overall, the simultaneous algorithm grows exponentially with dimension, whereas the sequential algorithm grows linearly.

Chapter 5

Results

The algorithms shown apply to different problems and are thus best used when used together. Both FFRED and OFPR can be shown to be special cases of the more general OSPR algorithm. Therefore, the results of OFPR and OSPR will be shown to illustrate the impact of operating the time dimension and the impact of sequential versus simultaneous operation for OSPR.

5.1 Metrics

While the projection of the constant modulus solution into orthogonal frequencies will reduce the PAPR, the extent to which it does is dependent on the following factors: the number of iterations that OFPR is allowed to run, the amount of power the algorithm will put into orthogonal frequencies, represented by $\%\beta_{\perp}$, and the number of orthogonal frequencies available, which is $b_{\perp} = N - b - 2a$. Therefore the results will examine a few metrics that will measure the efficacy and efficiency of OFPR. The PAPR is defined as

$$PAPR = \frac{\max |\mathbf{s}_i|^2}{\frac{1}{N}||\mathbf{s}_i||^2} \tag{5.1}$$

5.2 OFPR

The desired waveform $\mathbf{r}$ is an OFDM waveform with 4-QAM modulation of length $N = 1024$. Let $a = N/64 = 16$, and $b = \frac{5}{8}N$ so that $b_\perp = \frac{3}{8}N$. All results were averaged over 20000 iterations. The first figure will investigate the effect of $\%\beta_\perp$ on the reduction of PAPR. For this test, OFPR was ran for 100 iterations for each value of $\%\beta_\perp$. As one can see, the PAPR reduces with $\%\beta_\perp$, up to a value of $\%\beta_\perp = \%100$, at which point the PAPR has been reduced by 7 dB. This result demonstrates the decreasing difference between $\mathbf{s}_i$ and $\tilde{\mathbf{s}}_i$ with respect to $\%\beta_\perp$, and how given a certain value of $\%\beta_\perp$, $\tilde{\mathbf{s}}_i$ is more likely to be equal to $\mathbf{s}_i$.

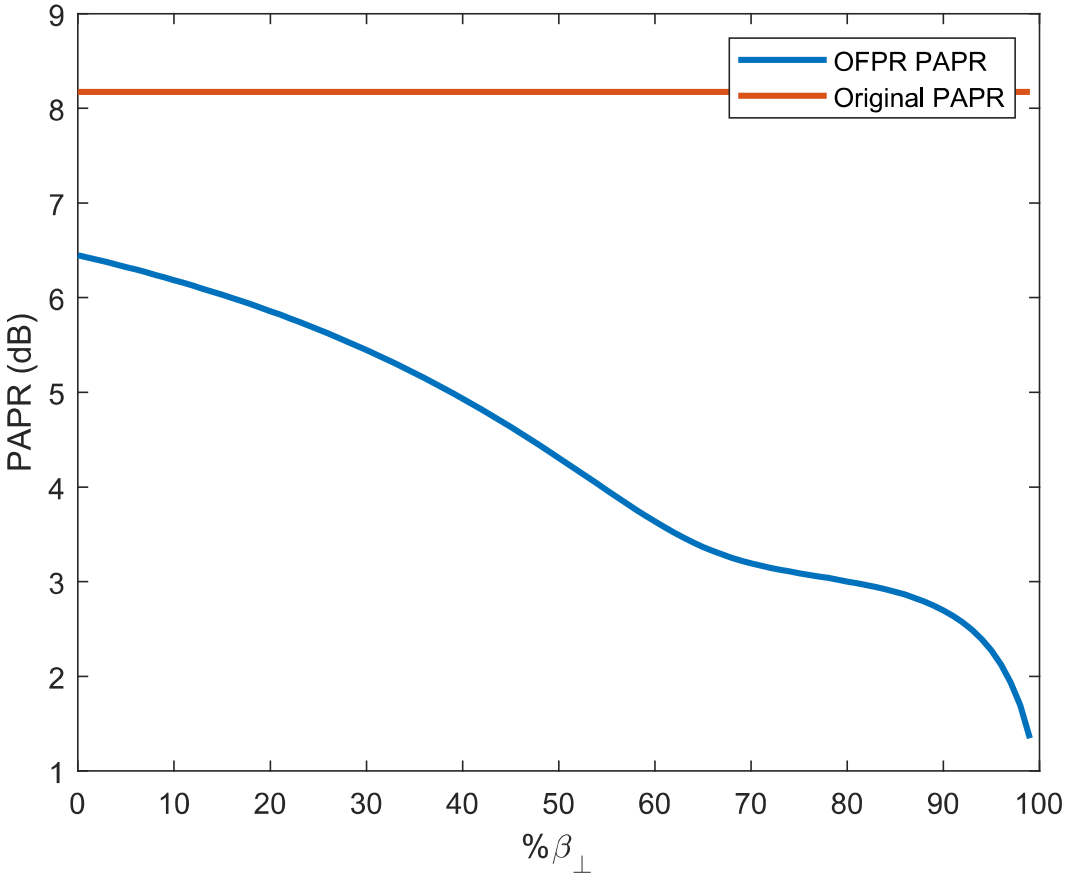

Figure 5.1: Peak-to-average Power Ratio versus $\%\beta_\perp$.

To further underline this point, the next figure investigates the RMS difference between the original transmit waveform and $\tilde{s}_i$ as a function of $\%\beta_\perp$. As one can see from Fig. 5.2, the RMS difference between the two waveforms decreases up to a point at which the increasing power of the out-of-band portion begins to leak into the in-band part and causes distortion. This distortion, combined with the decreasing efficiency of the algorithm with increasing $\%\beta_\perp$, shows that too high a selection of $\%\beta_\perp$ is harmful to efficiency and correctness. Therefore, one should take care when choosing the correct value of $\%\beta_\perp$, which depends on the required minimum error or efficiency. The bit error rate is the proportion of bits that differ after the signal has been received and decoded (in this case, the receive is identical to the transmit.) The figure shows the result of the constant modulus projection.

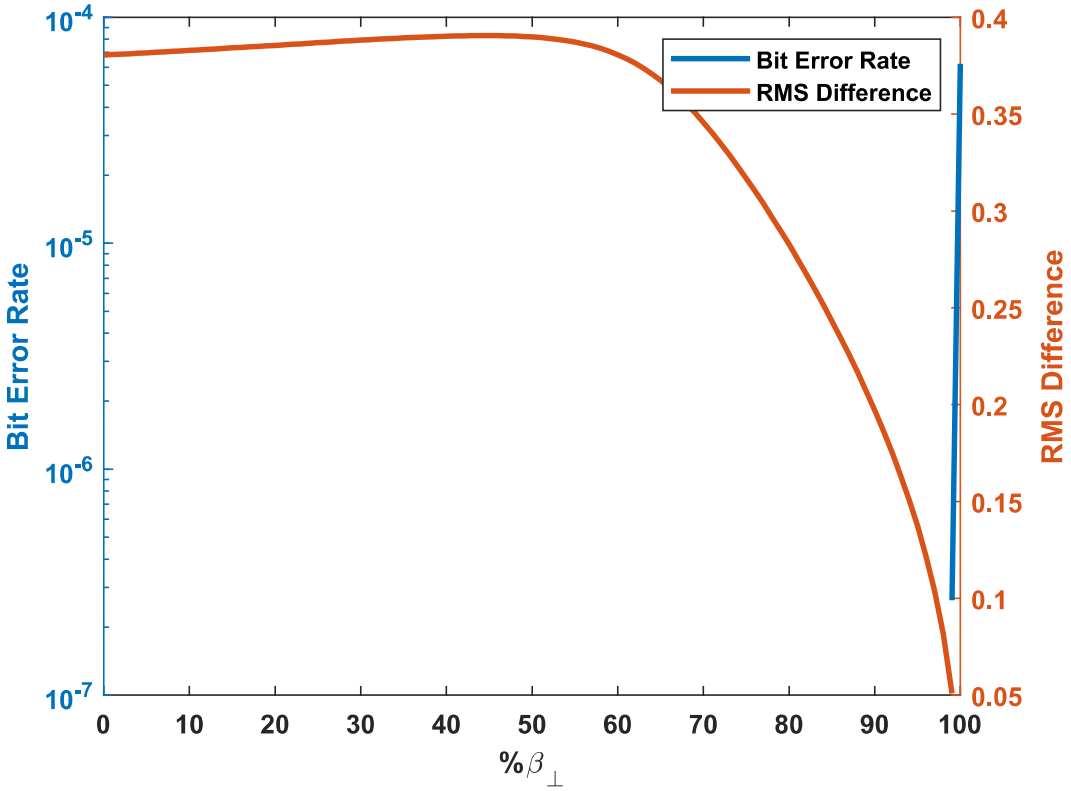

Figure 5.2: RMS Difference and Bit Error Rate vs $\%\beta_\perp$.

The following figure investigates the impact of the number of iterations on the PAPR of the OFPR waveform. As can be seen from Fig. 5.3, the algorithm has nearly converged (as much as possible) in only ten iterations. Such fast convergence demonstrates the usefulness of the algorithm for real-time applications. The figure also reflects the impact of $\%\beta_{\perp}$, as higher values lead to convergence to lower PAPRs.

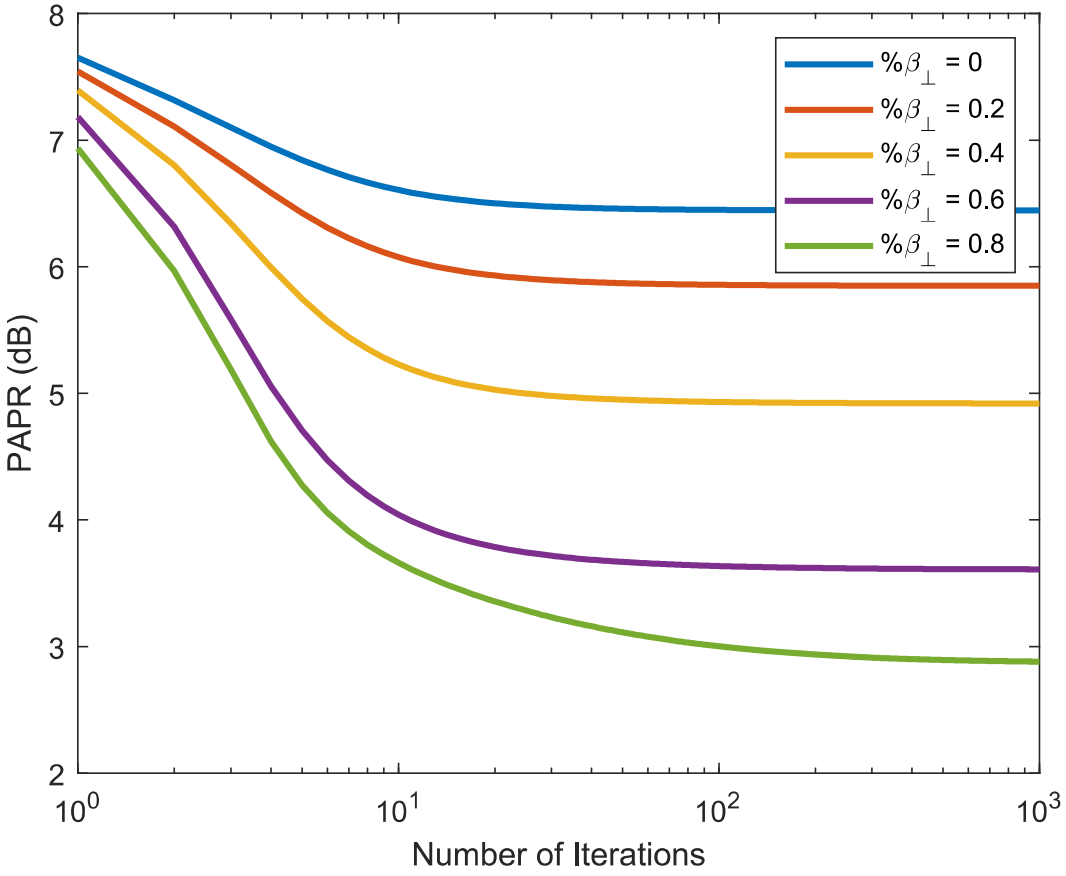

Figure 5.3: Peak-to-average Power Ratio versus Number of Iterations.

As the algorithm is utilizing the extra bandwidth outside of the original signal, the next figure examines the impact of the guard window (which reduces the outside bandwidth) on the reduction of PAPR. Intuitively, one would expect the efficacy to decrease with decreasing extra bandwidth available. As one can see from Fig. 5.4,

as the signal takes up more of the total bandwidth, the more the PAPR is reduced. The x-axis of the figure represents the total bandwidth of the signal as a percentage of the total possible. In other words, percentage bandwidth is the sum $b + b_{\perp}$. The graph begins at 62.5% since that is what the original signal occupies. The PAPR reduction increases with percent bandwidth because the initial b is fixed, and therefore an increase in percent bandwidth is equivalent to an increase of $b_{\perp}$

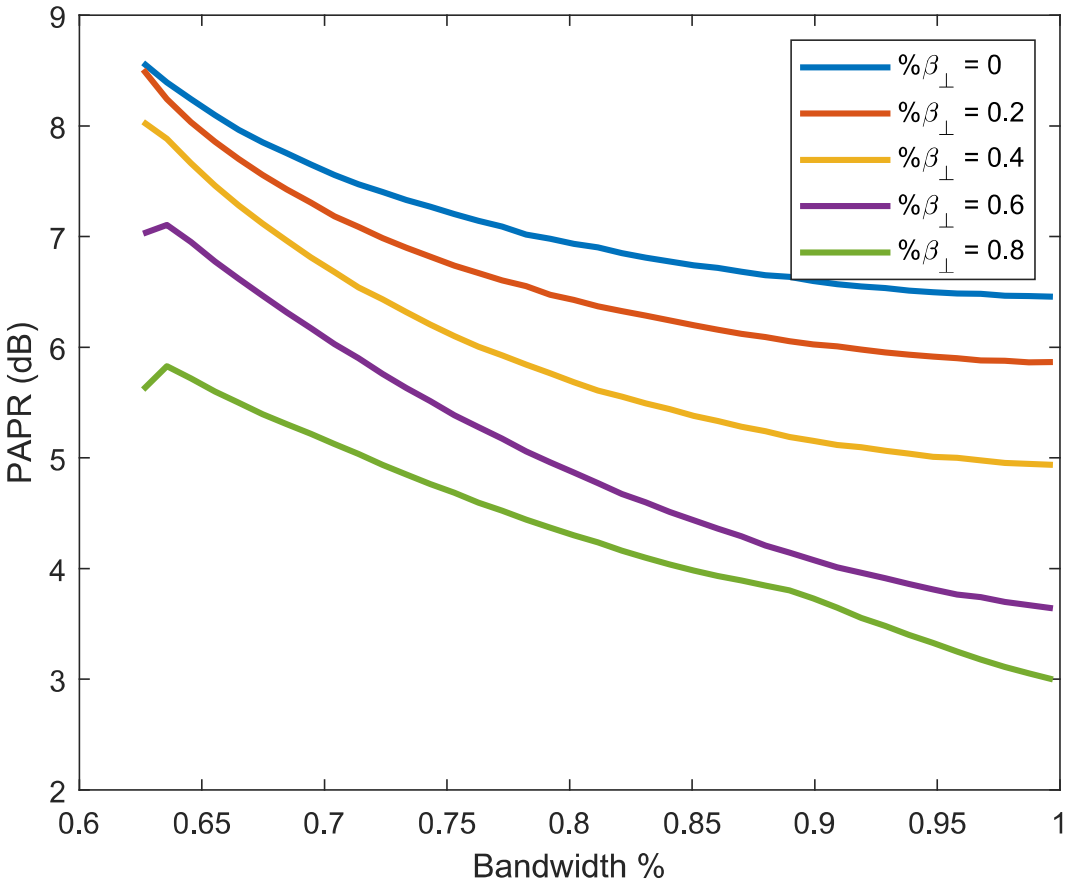

Figure 5.4: PAPR versus % Bandwidth.

The following figure examines the use of "empty" room in the spectrum of the signal of interest by investigating the spectral properties of a signal generated by OFPR. As one can see in Fig. 5.5, the extra power is placed entirely outside of the bandwidth of the original signal and is notched at the ends to avoid out-of-band

interference. The width of the notch at the ends is the guard window is represented by a. The OFPR and original waveform line up identically in the middle (the band of interest) as expected. One notes that the overall power of these two waveforms is different, since there is more spectral content in the OFPR waveform. This is on purpose, however, to illustrate the equality of the two waveforms in-band (after taking power into account), and to show the placement of the out of band power to ensure the signal is constant modulus.

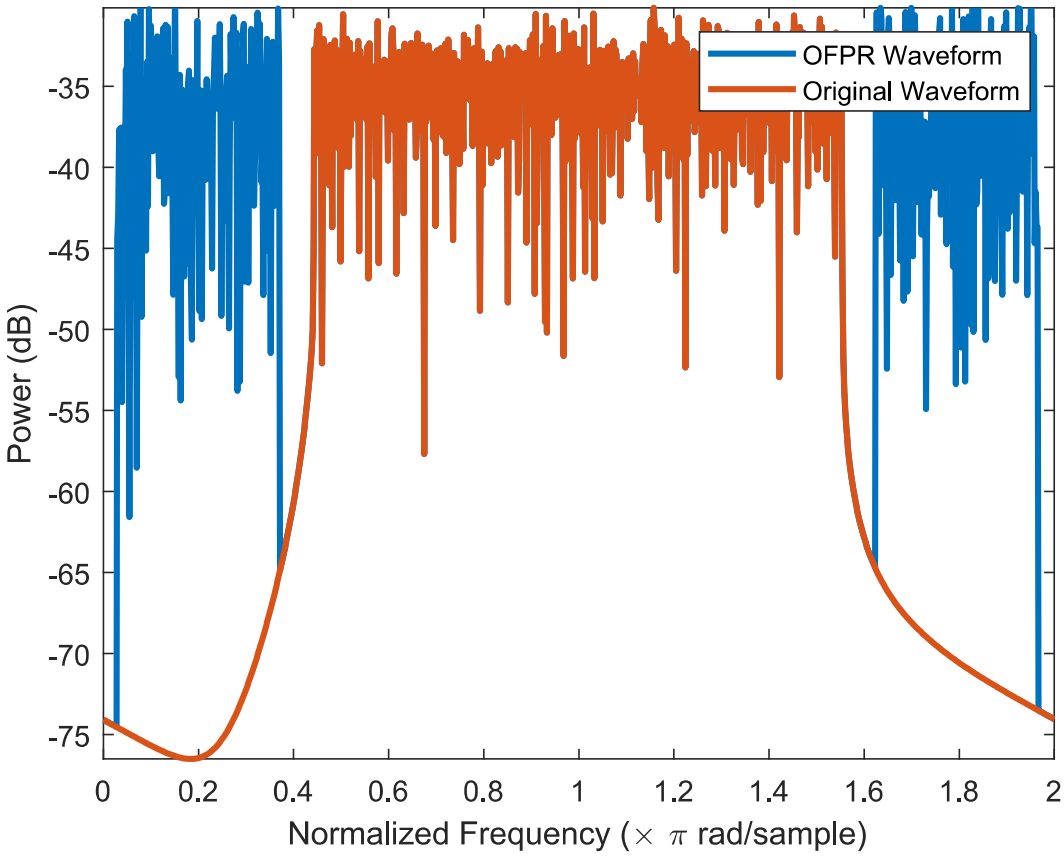

Figure 5.5: Spectra of original and OFPR signals.

Because the extra interference is out of band (in the case of $\mathbf{s}_i$) or is minimized within the band (in the case of $\tilde{\mathbf{s}}_i$), a simple bandpass filter can be used to avoid out of band emission. This step must occur after amplification, though, as the filtered

signal will no longer be constant modulus. As one can see from Fig. 5.6, filtering the signal significantly reduces the out-of-band interference since the spectral content of the communications signal is unaffected by the algorithm.

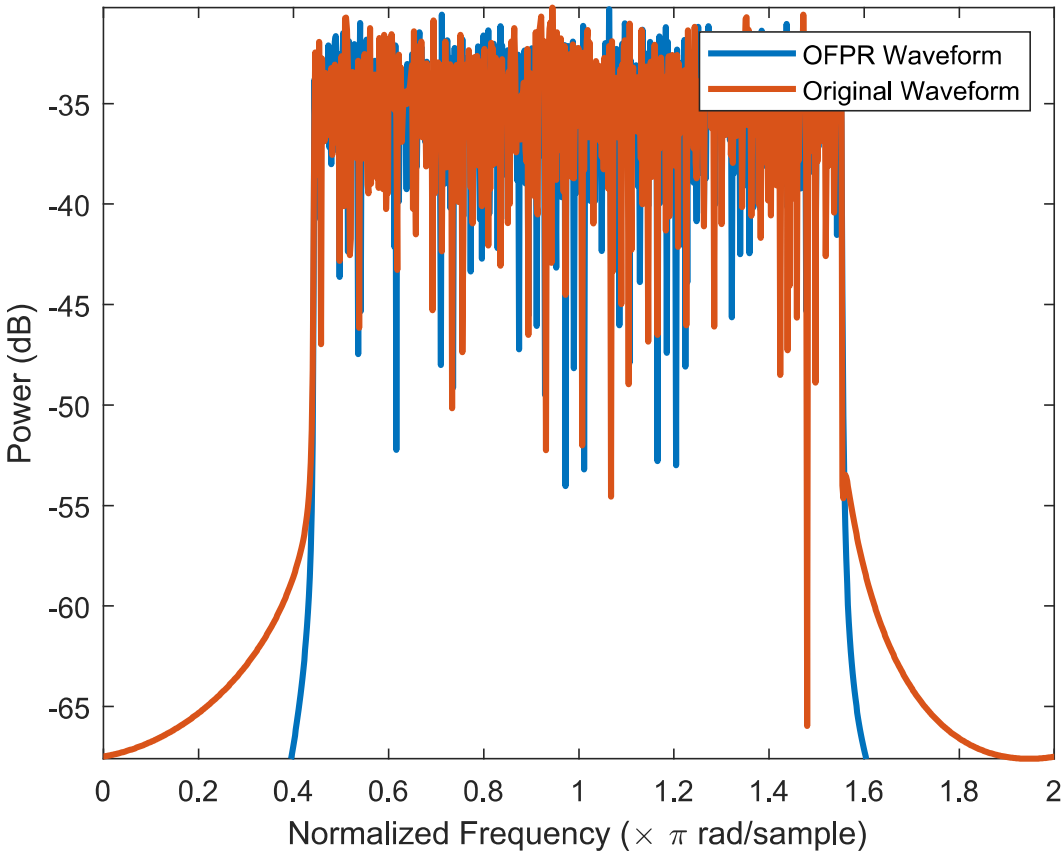

Figure 5.6: Spectra of original and filtered OFPR signals.

From [17], it is known that the efficiency of a class B amplifier is given by

$$\eta_a = Ge^{-g\gamma_{dB}} \tag{5.2}$$

Where $G = 90.7\%$ is the optimal efficiency of the amplifier, $g = 0.1202$ and γ_{dB} is the PAPR of the signal in dB. The portion of usable power of the OFPR waveform is defined as

$$\eta_{ofpr} = \frac{RMS(\mathbf{Ps})^2}{RMS(\mathbf{s})^2} \tag{5.3}$$

and the total efficiency is

$$\eta = \eta_a \eta_{ofpr} \tag{5.4}$$

Using this model, the increased efficiency of OFDM transmission is demonstrated as seen in Fig. 5.7. Three traces are shown. The blue trace is the final power efficiency of the converged OFPR algorithm after the constant modulus projection. The red trace is also the final power efficiency of the converged OFPR algorithm but is taken prior to the constant modulus projection. These two results are compared to the original OFDM signal, shown in the yellow trace. Shown also is that for high enough $\%\beta_{\perp}$, efficiency decreases to the point where the original waveform is more efficient to transmit. Also, it can be seen that the non-constant modulus result is less efficient than the original transmission. However, it is still of value when considering that the non-constant solution will provide a more accurate rendition of the desired signal than the constant modulus result. For most cases where one desires efficiency, the constant modulus is much more efficient than the original or non-constant modulus result.

5.3 OFPR and FFRED

The FFRED algorithm has demonstrated reducing the PAPR of a transmit waveform matrix by utilizing the orthogonal complement of spatial steering vectors. When using such a technique, the excess power required to make high PAPR signals constant modulus results in large spatial sidelobes and potentially reduced transmit power in the intended direction. Combining OFPR with these techniques can work in tandem and produce constant modulus signals with improved spatial and spectral containment. Consider the previous waveform being transmitted by a $M = 32$ element array, with element spacing $d = \frac{\lambda}{2}$. Consider a single beam transmit of the

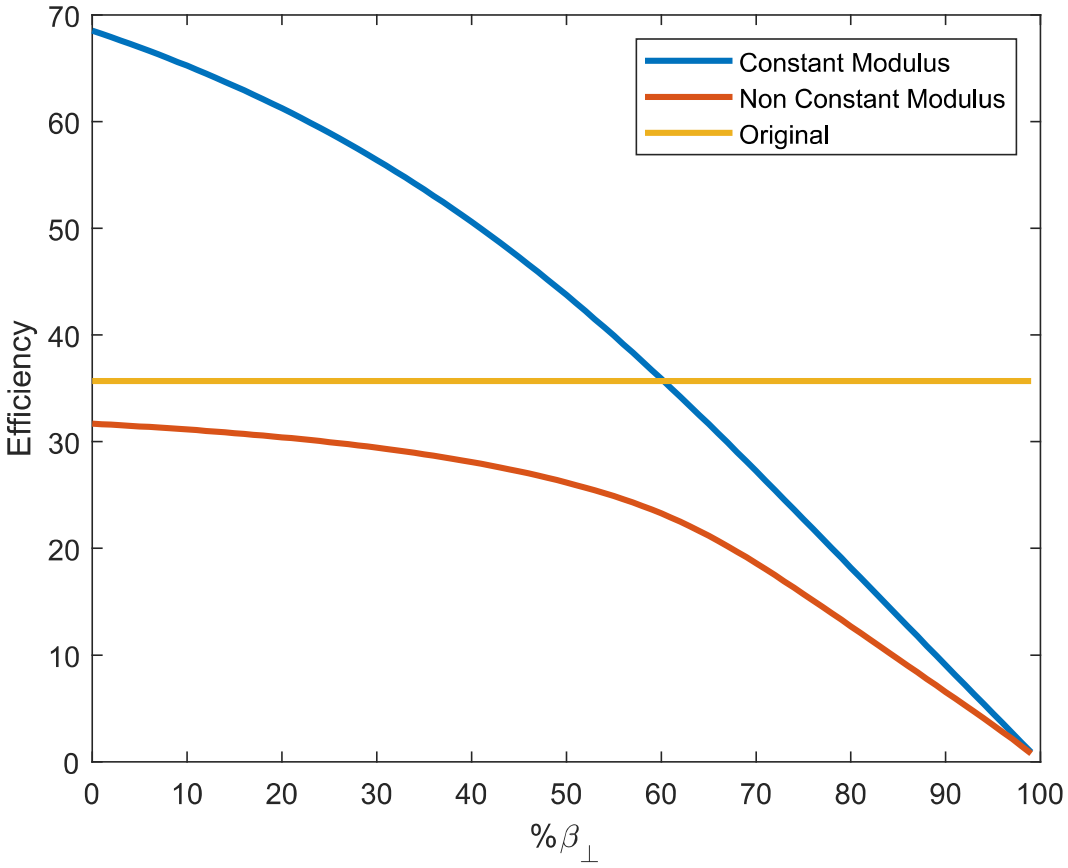

Figure 5.7: Efficiency of OFPR constant and non constant modulus results versus $\%\beta_\perp$

aforementioned OFDM signal towards $\theta_c = 15°$. Without OFPR, FFRED has large sidelobes, as can be seen in Fig. 5.8. This test was performed with 10^3 iterations of FFRED to ensure convergence. The next figure will investigate the impact that OFPR can have on the spatial spectrum of FFRED. The same test as before will be performed, but now the waveform is processed by OFPR before being used by FFRED, resulting in lower spatial sidelobes signal as seen in Fig. 5.8. This test was performed with $\%\beta_\perp = \%60$, at which point the efficiency is still greater than not using OFPR (as was shown in Fig. 5.7).

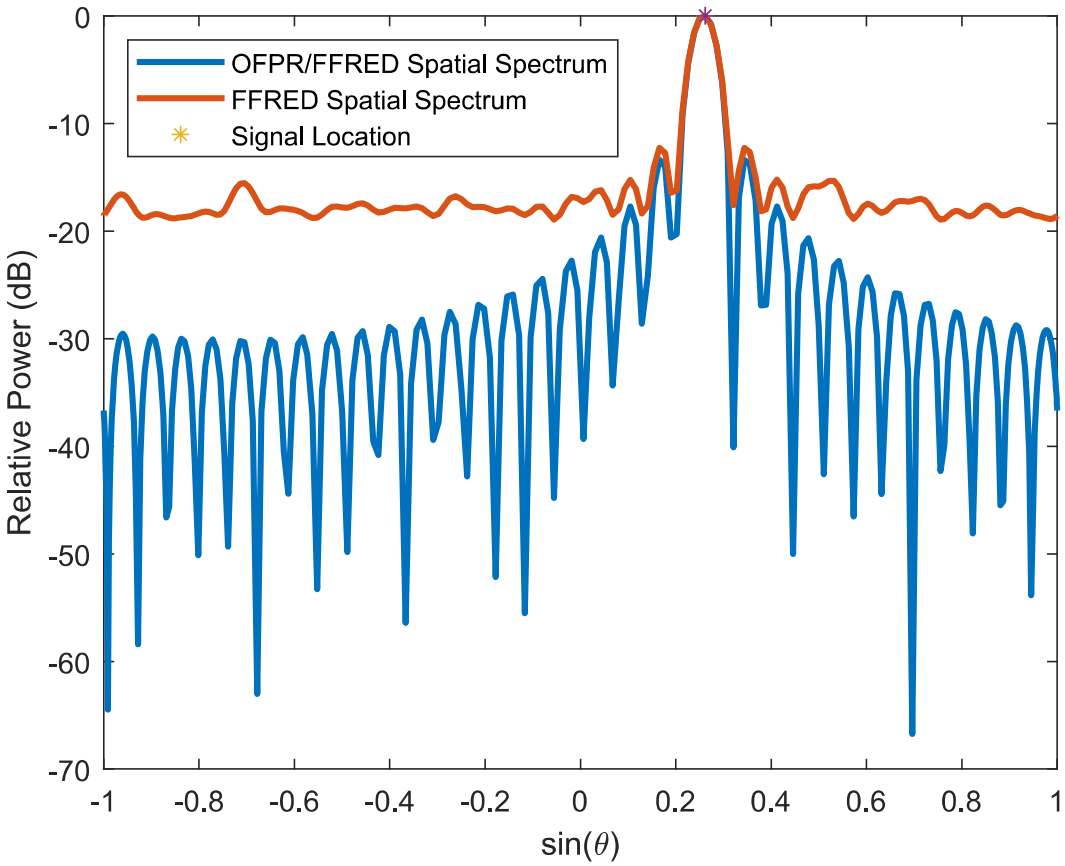

Figure 5.8: Spatial Spectrum of FFRED.

5.4 OSPR

In order to understand the difference between the simultaneous and sequential versions of OSPR, the results will first investigate the spatial-temporal frequency spectrum of each of the proposed methods (frequency domain versions of FFRED, OFPR, OSPR). The spatial-temporal spectrum consists of taking the two-dimensional Fourier transform of the resulting beamformed matrix. Consider the previous OFDM waveform of length $N = 2^{10} = 1024$. In the time domain, this waveform has a high PAPR, which can be seen in Fig. 5.9.

Using just OFPR alone will result in very good spatial characteristics (i.e., low

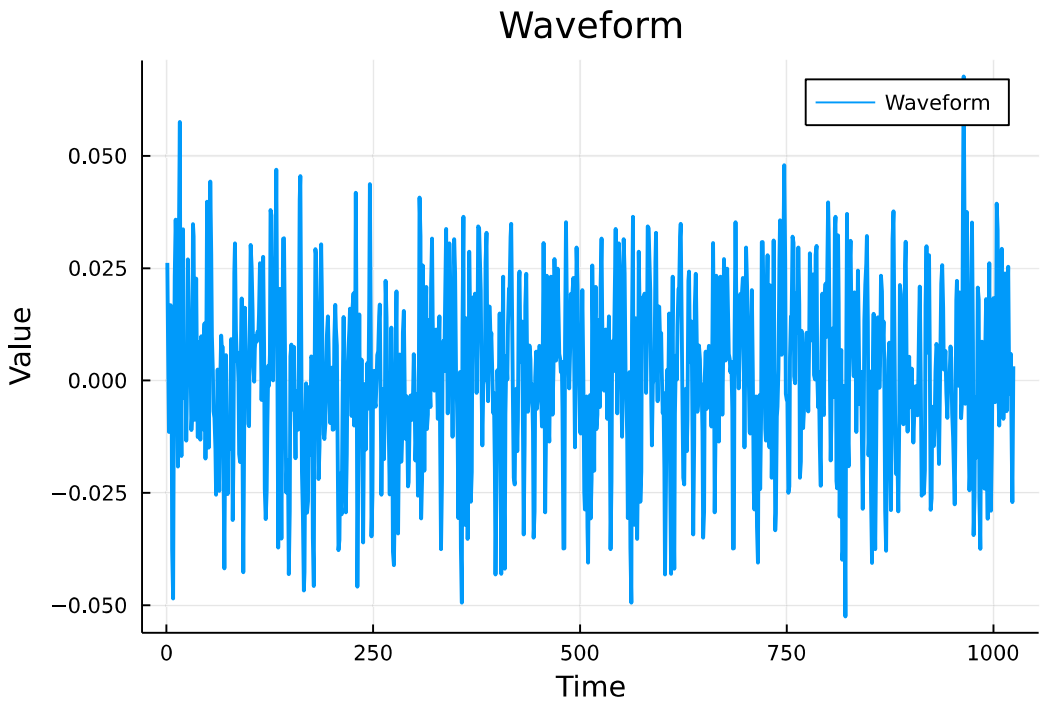

Figure 5.9: Specified waveform in the time domain.

sidelobes). However, the overall reduction of PAPR will be reduced. As one can see in Fig. 5.10, the spatial characteristics are indeed good. However, the underutilization of the spectrum results in a lower PAPR reduction than would be possible by utilizing the entire spatial-temporal spectrum (the PAPR reduction will be shown in a later graph).

To see the performance of the various algorithms in the direction of interest, one can take the results of the spatial-temporal spectrum and extract the vector along the direction of interest. Or, more formally,

$$\mathbf{g} = \mathbf{S}^H \mathbf{v} \tag{5.5}$$

where $\mathbf{S}$ is the result of the optimization, and $\mathbf{v}$ is the steering vector of the direction of interest. Fig. 5.11 shows the result for each of the algorithms as a function of

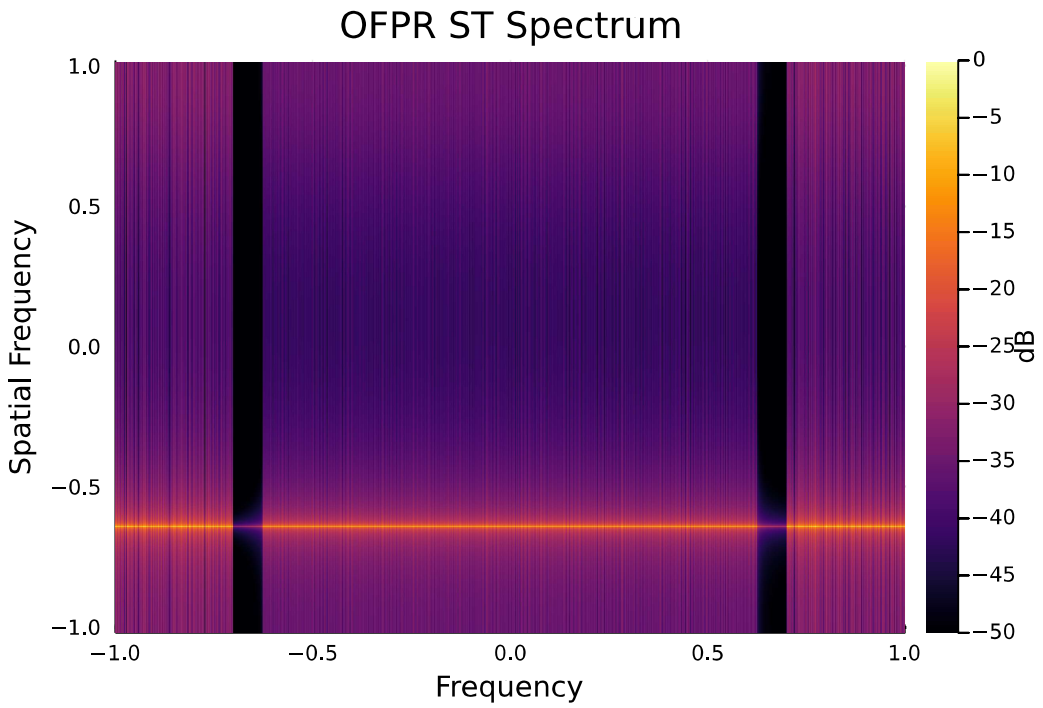

Figure 5.10: Spatial-temporal Spectrum of OFPR (i.e., the conventially beamformed results of OFPR).

the temporal spectrum (i.e., the Fourier transform of the time-domain signal in the direction of interest). One can also examine the waveform power as a function of steering angle. This figure shows the equivalent information as in Fig. 5.8, except that the number of array elements has changed in this case. Fig. 5.12 shows the best algorithm (in terms of spatial sidelobes) is OFPR since there is no utilization of the spatial orthogonal complement. The next best is sequential OSPR, followed by FFRED, and finally simultaneous OSPR. The simulated phased array that was used has $M = 2^{10} = 1024$ elements placed $d = \lambda/2$ apart. As one can see in Fig. 5.13, the FFRED algorithm has placed extra noise in the areas that are outside of the temporal spectrum of interest and the spatial spectrum of interest. This is good in the sense that the extra power will be orthogonal to the original waveform. However, underutilized parts of the spatial-temporal spectrum near the edges can

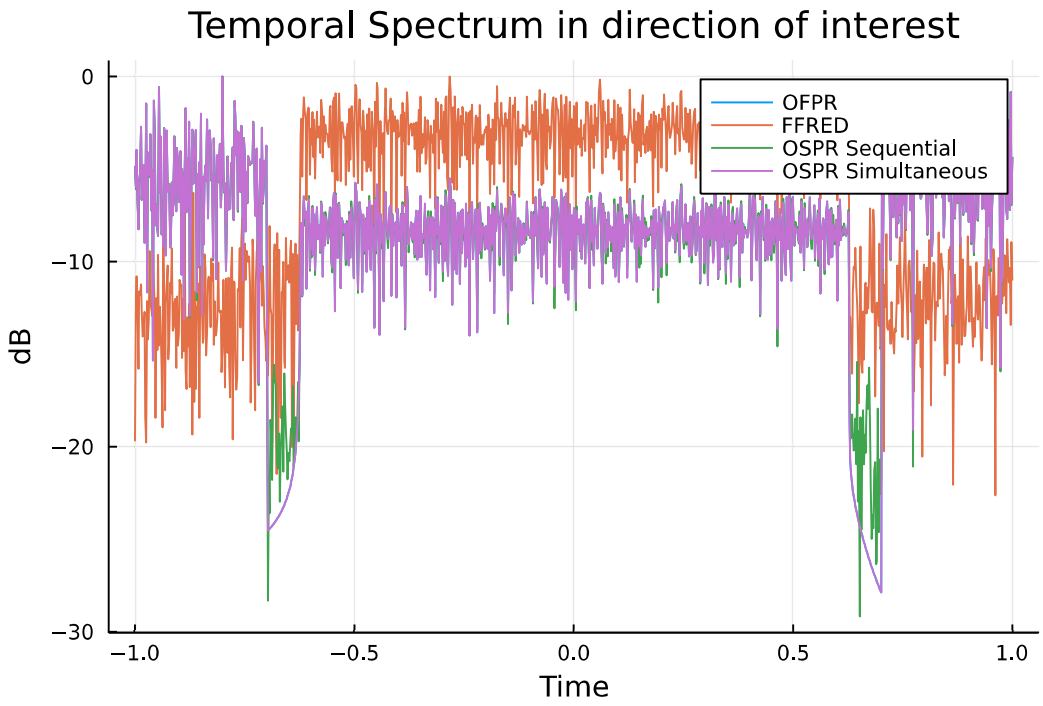

Figure 5.11: Temporal spectrum of the proposed algorithms in the direction of interest.

be seen. Since the spectrum of the original waveform is low in those regions, they will correspondingly be low in the FFRED processed spectrum.

In order to use the simultaneous version of OSPR, one must construct a spectral mask that will guarantee that the masking of any matrix will be orthogonal to the input matrix. In Fig. 5.14, one can see how the majority of the spatial-temporal spectrum is available for use, with the small dark region in the middle corresponding to the spatial-temporal spectrum of the original waveform.

In the simultaneous version of OSPR, one would expect that the extra spectral power would be placed in all parts of the spectrum which were not masked off by the mask. As one can see in Fig. 5.15, extra power is indeed present in all of the spatial-temporal spectrum, representing a full utilization of the available resources. By using the entire spectrum, the effect in any one dimension is reduced.

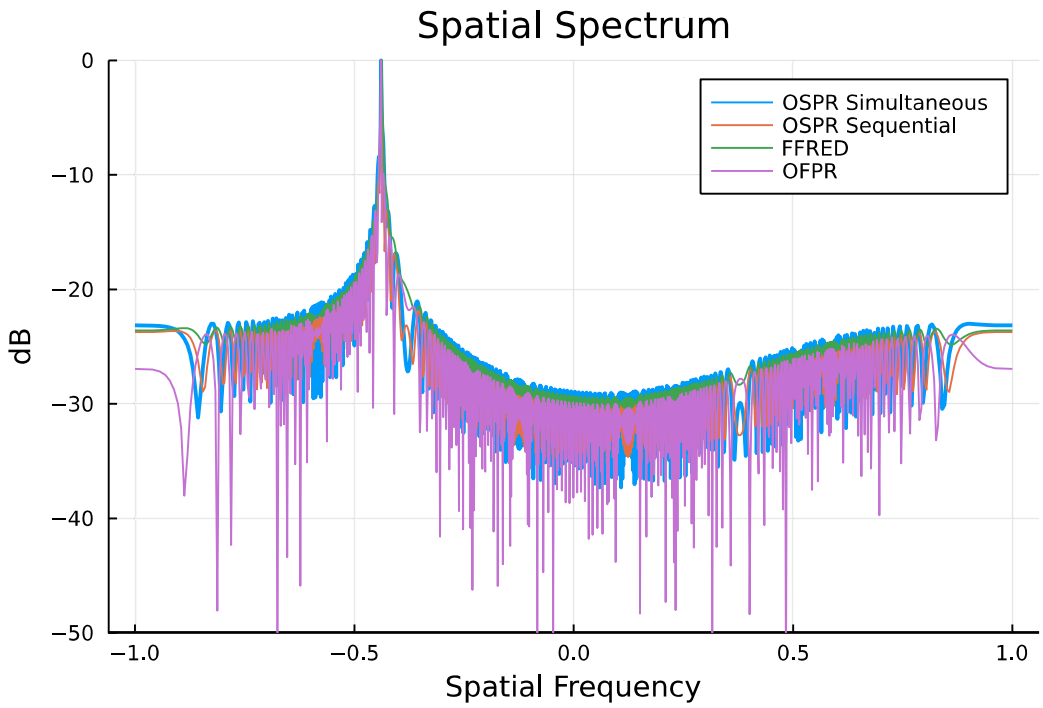

Figure 5.12: Spatial spectrum of the proposed algorithms in the direction of interest.

The sequential application of the OSPR algorithm has a much simpler structure than the simultaneous version. In Fig. 5.16, one can see that the overall extra spatial power is akin to the combination of the FFRED and OFPR powers rather than a full overall utilization. The edges of the spectrum are underutilized as in FFRED, but the extent to which they are underutilized is reduced since the OFPR waveform has higher temporal sidelobes.

Finally, one would like to see how much the PAPR is being reduced at each step of each algorithm. Fig. 5.17 presents this information. One notes that the OSPR sequential version starts at a lower PAPR than the rest of the algorithms; this is because the input to the algorithm is simply the OFPR waveform, which has a reduced PAPR. Since all the algorithms converge within the given window, the fact that this algorithm starts at a lower value has no consequence on the overall results.

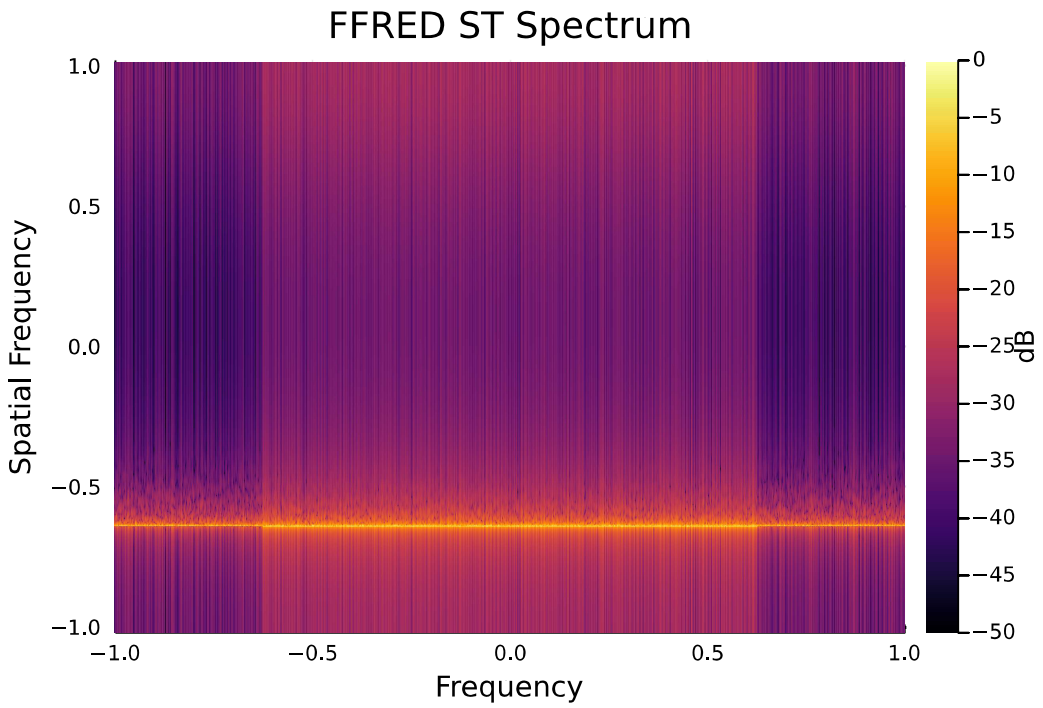

Figure 5.13: Spatial-temporal spectrum of FFRED.

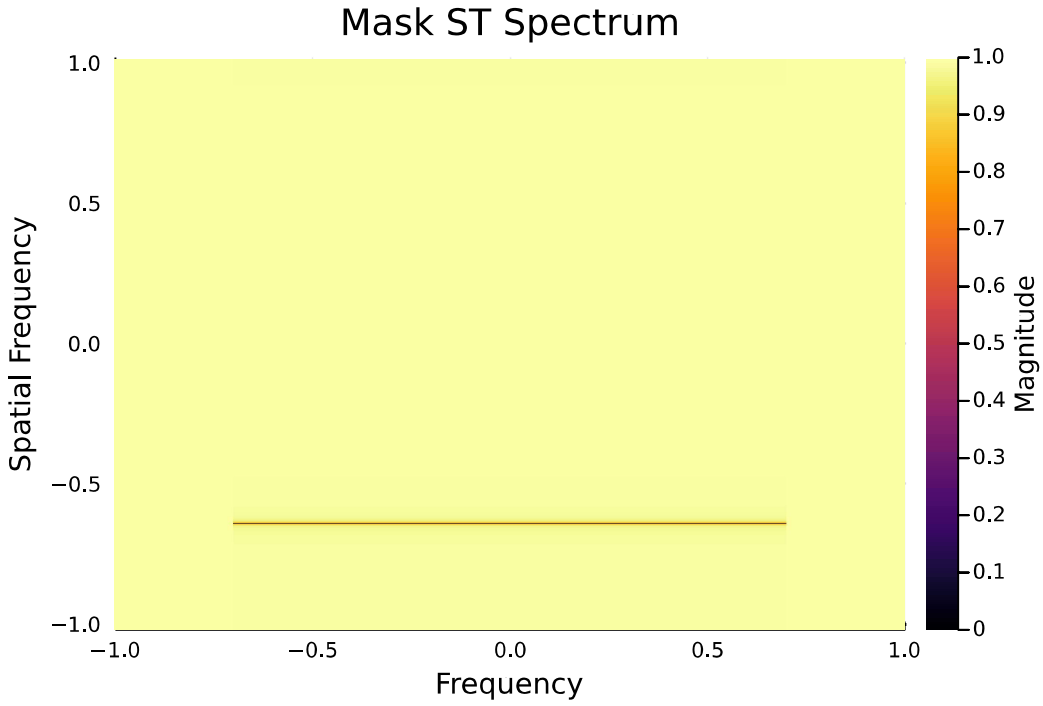

Figure 5.14: Spatial-temporal spectrum of the (frequency based) projection tensor.

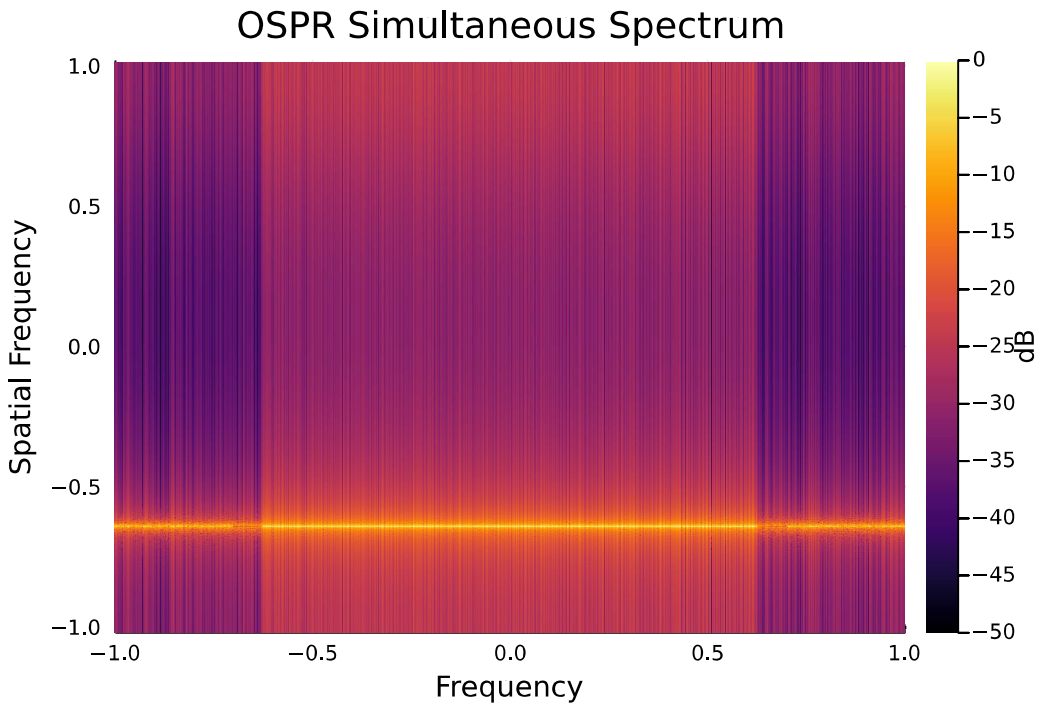

Figure 5.15: Spatial-temporal spectrum of simultaneous OSPR.

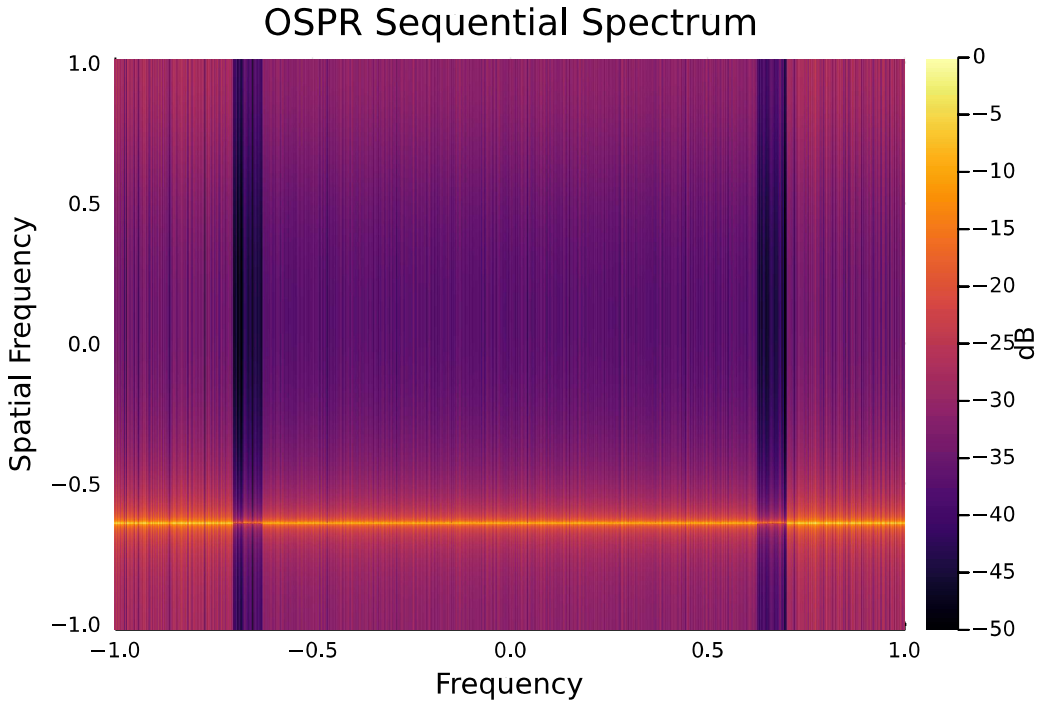

Figure 5.16: Spatial-temporal spectrum of sequential OSPR.

From the figure, one can see that the best overall performance is achieved using the OSPR sequential model. This does not line up with the author's expectation that the simultaneous version of OSPR would perform the best. In fact, the OSPR sequential version performs on the same level as FFRED, suggesting an underutilization of spectral resources that merits further investigation.

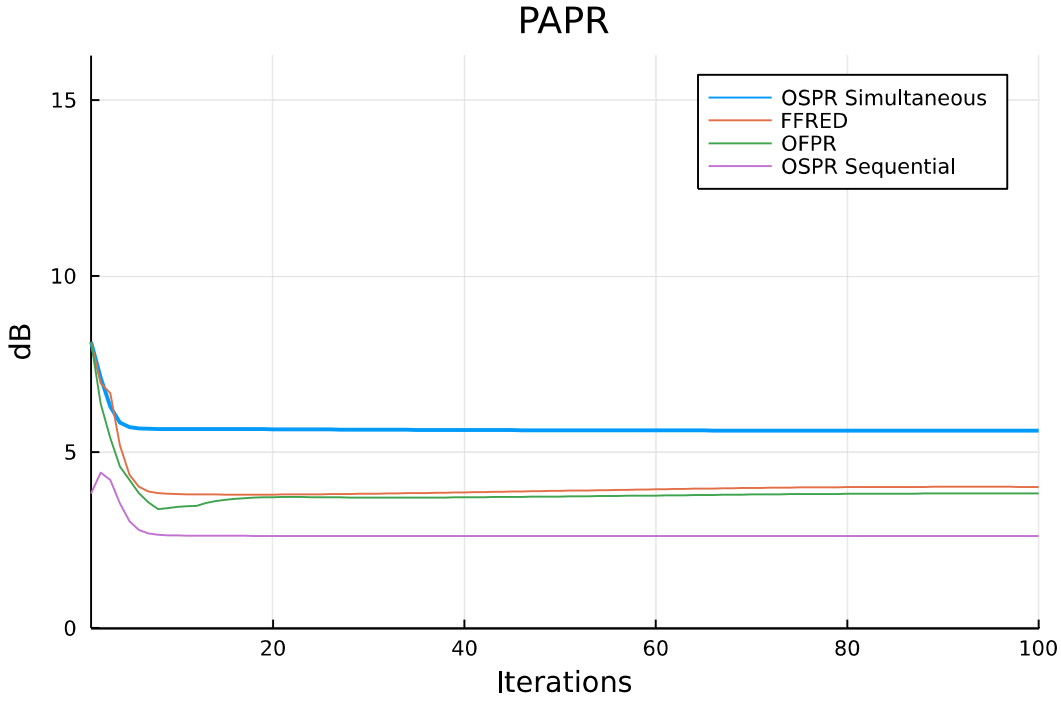

Figure 5.17: PAPR reduction for each iteration of the proposed algorithms.

5.5 Conclusion

Inspired by recent work [4, 5], two new methods of PAPR reduction for non-constant modulus waveforms have been developed, and two previous methods have been improved using fast vector rejection methods. The orthogonal complement of the waveform was used to reduce PAPR significantly. The effects of different parameters of OFPR were examined in conjunction with the use of FFRED. The

efficacy of OFPR and OSPR were demonstrated on waveforms with a high PAPR. For future work, optimal power distribution, i.e., the minimal combined power in spatial sidelobes and orthogonal frequencies to allow for the most efficient waveform design, will be explored. Also, the discrepancy between the simultaneous and sequential versions of OSPR will be investigated.

References

[1] B. Ravenscroft, P. M. McCormick, S. D. Blunt, E. Perrins, and J. G. Metcalf, "A power-efficient formulation of tandem-hopped radar amp; communications," in *Proc. IEEE Radar Conf. (RadarConf18)*, Apr. 2018, pp. 1061–1066.

[2] B. Ravenscroft, P. M. McCormick, S. Blunt, E. S. Perrins, C. Sahin, and J. G. Metcalf, "Experimental assessment of tandem-hopped radar and communications (thoracs)," in *2019 International Radar Conference (RADAR)*, 2019, pp. 1–6.

[3] P. M. McCormick, B. Ravenscroft, S. D. Blunt, A. J. Duly, and J. G. Metcalf, "Simultaneous radar and communication emissions from a common aperture, part ii: Experimentation," in *Proc. IEEE Radar Conf. (RadarConf)*, May 2017, pp. 1697–1702.

[4] P. M. McCormick, S. D. Blunt, and J. G. Metcalf, "Simultaneous radar and communications emissions from a common aperture, part i: Theory," in *Proc. IEEE Radar Conf. (RadarConf)*, May 2017, pp. 1685–1690.

[5] P. M. McCormick, C. Sahin, S. D. Blunt, and J. G. Metcalf, "Physical waveform optimization for multiple-beam multifunction digital arrays," in *Proc. and Computers 2018 52nd Asilomar Conf. Signals, Systems*, Oct. 2018, pp. 1036–1041.

[6] K. Yang, G. I. Haddad, and J. R. East, "High-efficiency class-a power amplifiers with a dual-bias-control scheme," *IEEE Transactions on Microwave Theory and Techniques*, vol. 47, no. 8, pp. 1426–1432, 1999.

[7] K. W. Whites, "Lecture 18: Common emitter amplifier. maximum efficiency of class a amplifiers. transformer coupled loads." Lecture Notes, 2006.

[8] T. S. Gray, *Amplifiers with Operation Extending beyond the Linear Range of the Tube Characteristic Curves; Class AB, Class B, Class C Amplifiers*, 1954, pp. 609–656.

[9] J. Jakabosky, B. Ravenscroft, S. D. Blunt, and A. Martone, "Gapped spectrum shaping for tandem-hopped radar/communications amp; cognitive sensing," in *2016 IEEE Radar Conference (RadarConf)*, 2016, pp. 1–6.

[10] J. Jakabosky, S. D. Blunt, and B. Himed, "Waveform design and receive processing for nonrecurrent nonlinear fmcw radar," in *2015 IEEE Radar Conference (RadarCon)*, 2015, pp. 1376–1381.

[11] D. Youla, "Generalized image restoration by the method of alternating orthogonal projections," *IEEE Transactions on Circuits and Systems*, vol. 25, no. 9, pp. 694–702, 1978.

[12] D. C. Youla and H. Webb, "Image restoration by the method of convex projections: Part 1 - theory," *IEEE Transactions on Medical Imaging*, vol. 1, no. 2, pp. 81–94, 1982.

[13] J. R. Fienup, "Phase retrieval algorithms: a comparison," *Applied optics*, vol. 21, no. 15, pp. 2758–2769, 1982.

[14] A. Levi and H. Stark, "Image restoration by the method of generalized projections with application to restoration from magnitude," in *ICASSP '84. IEEE International Conference on Acoustics, Speech, and Signal Processing*, vol. 9, 1984, pp. 88–91.

[15] H. H. Bauschke, P. L. Combettes, and D. R. Luke, "Phase retrieval, error reduction algorithm, and fienup variants: a view from convex optimization," *JOSA A*, vol. 19, no. 7, pp. 1334–1345, 2002.

[16] L. K. Patton and B. D. Rigling, "Phase retrieval for radar waveform optimization," *IEEE Transactions on Aerospace and Electronic Systems*, vol. 48, no. 4, pp. 3287–3302, 2012.

[17] D. Wulich, "Definition of efficient papr in ofdm," *IEEE Communications Letters*, vol. 9, no. 9, pp. 832–834, 2005.